UNIVERSITY OF
BIRMINGHAM

ASSESSMENT OF LIPID NANOCAPSULES AND LIPOSOMES AS NANOCARRIERS FOR C6 CERAMIDE DELIVERY TO BREAST CANCER CELLS

by

FRANSISKA CHRISTYDIRA SEKARINGTYAS

A thesis submitted to the University of Birmingham for the degree of

MASTER OF SCIENCE (MSc) by Research

SCHOOL OF PHARMACY

INSTITUTE OF CLINICAL SCIENCES

COLLEGE OF MEDICAL AND DENTAL SCIENCES

UNIVERSITY OF BIRMINGHAM

September 2023

ABSTRACT

Ceramides, a class of bioactive sphingolipids, have been shown to contribute to various cellular and signalling events. C6, as a short-chain ceramide, is considered the most potent ceramide which can inhibit proliferation and induce pro-apoptotic effects in specific cancer cells, including triple-negative breast cancer (TNBC). However, the therapeutic application of ceramides is limited due to their poor water-solubility and susceptibility to enzymatic degradation. Therefore, encapsulating ceramides into nanoparticles may be required to increase intracellular levels and generally enhance ceramide efficacy. This study investigates the use of lipid nanocapsules (LNCs) as a suitable alternative to liposome for ceramide delivery. The presence of C6 ceramide had no major impact on the physico-chemical properties of LNCs, but did affected liposome properties. LNCs formulations had greater stability under storage (at 4°C) and cell culture conditions than liposomes. Also, liposomes were more likely to aggregate at high salt concentrations. C6 ceramide-loaded nanoparticles (LNCs-C6 and liposome-C6) were more cytotoxic than equivalent ghost nanoparticles (LNCs-ghost and liposome-ghost) towards MDA-MB-231 breast cancer cells. C6 ceramide was confirmed to induce cancer cell death through apoptosis and caspase-3/7 activation. Encapsulating ceramide did not limit its pharmacology activity on TNBC cells, and in some cases mildly enhanced its efficacy with LNCs-C6 seen to be slightly more effective than liposome-C6. These results provide further insight into the application of LNCs as a compatible nanocarrier for ceramide delivery and offer a viable platform for future development of anticancer drug-loaded ceramide LNCs for combination therapy in cancer treatment.

ACKNOWLEDGEMENTS

First, I would like to express my heartily grateful to my supervisor, Dr Marie-Christine Jones, for her great guidance and valuable advice which encouraged me to build my critical thinking in research. I would also like to thank my second supervisor, Dr Hanene Ali-Boucetta.

Many thanks and huge appreciation to all my colleagues in Pharmacy Research Laboratory, especially Ilay Sema Ünal and Dr Sarah Gordon, for their generous assistance and encouragement in many moments during my research project.

I would also like to express my biggest gratitude to Indonesia Endowment Fund for Education (LPDP RI) for the financial sponsorship during my study at the University of Birmingham.

Finally, last but not least, I would like to give my special thanks to my dearest parents, sister and my best friend for their endless love and support throughout my life.

List of Abbreviations

BCRP	*Breast cancer resistance protein*
CCK8	*Cell-counting kit 8*
CDase	*Ceramidase*
CerS	*Ceramide synthase*
DES	*Dihydroceramide desaturase*
DH-CerS	*Dihydroceramide synthase*
DLS	*Dynamic light scattering*
DMEM	*Dulbecco's Modified Eagle Medium*
DMSO	*Dimethyl sulfoxide*
DNA	*Deoxyribonucleic acid*
DPBS	*Dulbecco's phosphate buffer saline*
DSPC	*1,2-distearoyl-sn-glycero-3-phosphocholine*
DSPE	*1,2-distearoyl-sn-glycero-3-phosphoethanolamine*
ER	*Oestrogen receptor*
FBS	*Foetal bovine serum*
HER2	*Human epidermal growth factor receptor*
HI	*Heat inactivated*
HLB	*Hydrophilic-lipophilic balance*
HS	*Hydroxystearate*
LNC	*Lipid nanocapsule*
LoD	*Limit of detection*
LoQ	*Limit of quantification*
MWCO	*Molecular weight cut-off*

MDR	*Multidrug resistance*
MPS	*Mononuclear phagocyte system*
PBS	*Phosphate buffer saline*
PdI	*Polydispersity index*
PEG	*Polyethylene glycol*
PI	*Propidium iodide*
P-gp	*P-glycoprotein*
PR	*Progesterone receptor*
PS	*Phosphatidylserine*
ROS	*Reactive oxygen species*
S1P	*Sphingosine-1-phosphate*
S1PP	*Sphingosine-1-phosphate phosphatase*
SAT	*Salt aggregation test*
SD	*Standard deviation*
SK	*Sphingosine kinase*
SMase	*Sphingomyelinase*
SMS	*Sphingomyelin synthase*
SPC	*Soybean phosphatidylcholine*
SPT	*Serine palmitoyl transferase*
STS	*Staurosporine*
TNBC	*Triple-negative breast cancer*
WST-8	*Water-soluble tetrazolium-8*
ZP	*Zeta potential*

Table of Contents

List of Figures

List of Tables

1. Introduction

1.1. Ceramide structure and synthesis

Ceramides are amphiphilic molecules, part of the sphingolipid family. Ceramides share a basic chemical structure consisting of a 18-carbon long sphingoid hydrophobic backbone with hydroxyl groups found on C1 and C3 carbons, a trans double bond across C4 and C5, and an amide linker at C2 (1,2) (Figure 1.1 A). Ceramides are categorised by the length of the *N*-acyl chain, which also dictates their biological activities (1,3). Ceramides with an acyl chain length between 14 and 26 are the main ceramides found in mammalian cells (1,4); high concentrations of these ceramides can be found in the stratum corneum where they help fulfil the barrier function of the skin (5,6). In contrast, shorter-chain ceramides (<C12) are absent or only exist in very low levels in the cell membranes (4,5), yet regulate important cellular responses and signalling pathways, in both normal and cancer (2,6,7).

In the body, ceramide levels are regulated by different metabolic pathways, including *de novo* synthesis, salvage pathway, and sphingomyelin hydrolysis (8–11). Firstly, *de novo* synthesis (Figure 1.1 B) produces ceramides through the condensation of serine and palmitoyl coenzyme A. Alternatively, ceramide synthesis can occur *via* the salvage pathway (Figure 1.1 C) which involves recycling sphingosine generated from the deacetylation of ceramides (>C12) by ceramidase (CDase); this pathway is also under the control of ceramide synthase (CerS) (10). The type of ceramide synthesised depend on which CerS enzyme (CerS1-CerS6) is involved. For example, CerS1 and CerS4 generate C18 – C20 ceramides, CerS5 and CerS6 generate C14 – C16 ceramides, CerS2 generates C22 – C24 ceramides, and CerS3 generates C28 – C32 ceramides (10,12). Moreover, ceramides are also generated

through the sphingomyelin pathway (Figure 1.1 D) from hydrolysis of sphingomyelin, a major component of plasma membrane (11,13), by sphingomyelinase to produce ceramides.

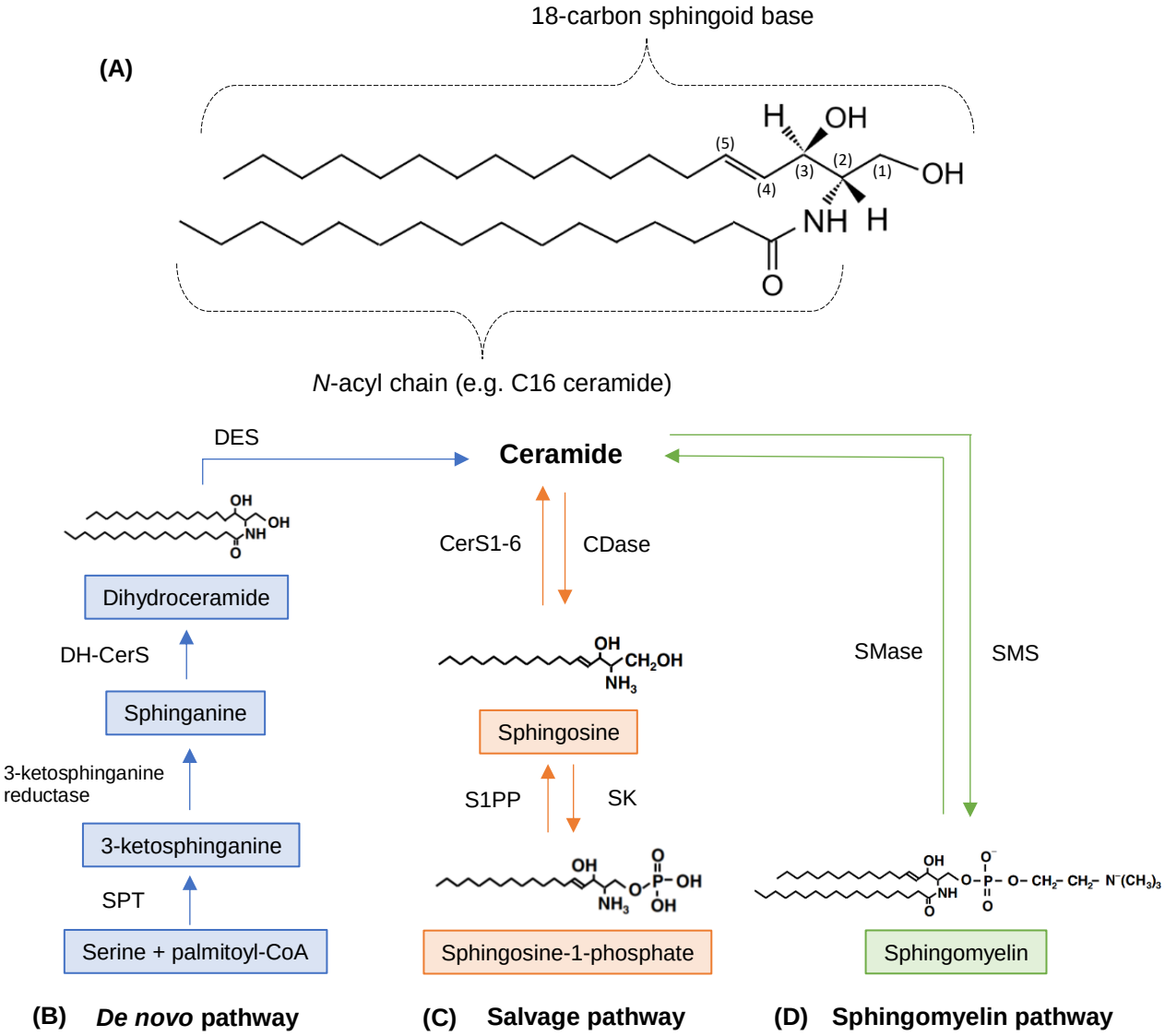

Figure 1.1. Structure of a ceramide molecule (A) adapted from (1) with permission from Elsevier. Ceramide synthesis through three main metabolic pathways: *de novo* (B), salvage (C), and sphingomyelin (D) adapted from (13) with modification and permission from Elsevier.

In terms of metabolism, ceramides can be hydrolysed by CDase to produce sphingosine which is then phosphorylated to produce sphingosine-1-phosphate (S1P) (10,14). Although ceramide and sphingosine are both part of the sphingolipid family they

have opposite functions in cancer. Ceramides regulate cell death and suppress tumour growth, whereas S1P promotes cell and tumour proliferation (10,15). Because of the complexity of sphingolipid activity, the right balance between ceramides and S1P must be achieved (15,16).

1.2. Role of ceramide in cancer

As previously mentioned, ceramides are bioactive sphingolipids that play an essential role in cell differentiation and senescence. This makes ceramides an interesting target for cancer therapy, especially as synthesis is often suppress in cancer cells (14,17). The exogenous administration of ceramides have been shown to trigger apoptosis in cancer cells (Table 1.1) (8,9,12,18); similarly, it was reported that anticancer drugs, such as cisplatin, vincristine and doxorubicin, could increase ceramide levels in specific cancer cells which could enhance their anti-cancer activity (19–21). The cellular functions of ceramides are acyl chain length- and cell type-dependent (22,23). It can be observed that short-chain ceramides (C2, C6, C8 ceramide) are more common in research than longer chain ceramides. Though ceramides, like phospholipids, are amphiphilic, the longer the alkyl chain, the more hydrophobic the ceramide (24,25), the more challenging the formulation becomes (26). Additionally, short-chain ceramide may be a substrate for ceramide synthesis to produce long-chain ceramides which makes them more interesting candidates as anti-cancer drugs (27,28).

Table 1.1. The use of ceramides in nanomedicine for cancer treatment

Ceramide	Cancer cells	Effect	Literature
C2 ceramide	Melanoma cells (B16F10, A375)	Pro-apoptotic	(29)
	Acute myeloid leukaemia (AML)	Pro-apoptotic	(30)
C6 ceramide	Breast cancer cells (MDA-MB-231, MDA435/LCC6, MCF-7)	Pro-apoptotic	(31–35)
	Cervical cancer cells (HeLa)	Inhibit proliferation	(36)
	Colon cancer cells (HCT116)	Pro-apoptotic	(37)
	Pancreatic cancer cells (PANC-1)	Pro-apoptotic	(38,39)
	Hepatocellular carcinoma (SK-HEP-1)	Pro-apoptotic	(40)
	Chronic lymphocytic leukaemia (JVM3)	Inhibit proliferation	(41)
C8 ceramide	Breast cancer cells (MDA435/LCC6)	Inhibit proliferation	(33)
C16 ceramide	Breast cancer cells (MCF-7)	Inhibit proliferation	(42)
	Leukaemia cells (HL-60)	Inhibit proliferation	(42)
	Cervical cancer cells (HeLa)	Pro-apoptotic	(43)

Among short-chain ceramides, C6 (Figure 1.2) is considered the most potent ceramide and can inhibit proliferation and/ or induce apoptosis in specific cancer cells, including breast, colon, hepatocellular and pancreatic cancer (31,33,37–40,44). Specifically, in breast cancer cells, shorter-chain ceramides exhibit stronger chemotherapeutic activity than the longer-chains (10,15,33,45). For instance, Shabbits *et al*. (33) reported that the IC50 of C6 (2.71 μM) and C8 ceramide (7 μM), in MDA435/LCC6 breast cancer cells was noticeably lower than for C10 (44.10 μM), C14 and C16 (>100 μM) ceramides. In addition, C6 ceramides were able to induce apoptosis in MDA-MB-231 breast cancer cells by upregulating caspase-3/7 activity (16,31,34).

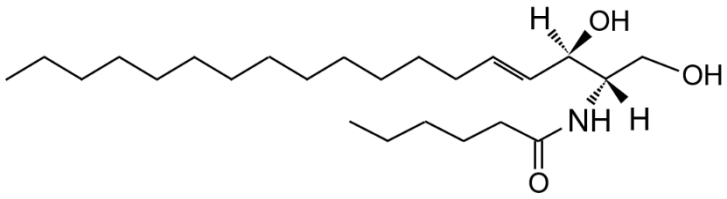

Figure 1.2. Chemical structure of C6 ceramide (N-hexanoyl-D-erythro-sphingosine)

The role of ceramides in breast cancer is the subject of growing interest, with current research evaluating the possibility of targeting the sphingolipid pathway to increase ceramide levels and promote ceramide-mediated cell death (46–48). This approach would be particularly attractive for triple-negative breast cancer (TNBC) where ceramides may act synergistically with anticancer drugs, as shown in MDA-MB-231 TNBC cells, when C6 ceramide was combined with docetaxel, doxorubicin, paclitaxel, or sorafenib (49–54).

Despite their potential role in tumour inhibition, the therapeutic application of ceramides may be limited due to limited water-solubility and susceptibility to enzymatic degradation (31,38,49), even for less hydrophobic C6 ceramide. C6 ceramide has poor aqueous solubility (slightly soluble in aqueous buffers), though it can be dissolved in DMSO (solubility >20 mg/mL) or ethanol (solubility >33 mg/mL) (12,31). Therefore, encapsulating ceramides into nanoparticles may be required to increase intracellular levels, protect against degradation, and enhance specificity towards cancer cells. Previously, liposomes have been widely used for that purpose, in part due to the similarities between phospholipids and sphingolipids (55,56) and the ability of ceramides to position themselves within the liposomal membrane (41,57,58).

1.3. Liposome and other ceramide delivery systems

Liposomes are spherical drug carriers prepared from one or more phospholipids with a water-filled inner core surrounded by one or more lipid bilayers (55,59). Although they are mostly used to encapsulate water-soluble drugs, liposomes can be used to deliver a variety of drugs. As such, liposomes are versatile, biodegradable, biocompatible drug carriers, and one of the few nanomedicines to have reached the clinic (56,60–62).

Table 1.2. Composition of C6 ceramide-loaded liposomes previously reported

Composition	mol%	Results
DSPC/ DOPE/ PEG(2000)-DSPE/ PEG(750)-C8 ceramide/ C6 ceramide	37.5/ 17.5/ 7.5/ 7.5/ 30	- IC50 5 μM (MDA-MB-231 cells) - Liposomes enhanced cytotoxicity and apoptosis induction, compared to free-C6 ceramide.
EPC/ Cholesterol/ PEG(2000)-DSPE/ C6 ceramide	70/ 15/ 3/ 15	- IC50 >200 μM (HeLa) - Liposome-C6 did not significantly induce apoptosis
DSPC/ Cholesterol/ C6 ceramide	40/ 45/ 15	- IC50 15.9 μM (MDA435/LCC6) - Liposome formulations did not enhance cytotoxicity of C6 ceramide.

It has been widely reported that C6 ceramide-loaded liposomes could be effective as an adjuvant cancer treatment that inhibits tumour growth (34–38). The lipid composition used for C6 ceramide-loaded liposomes in previous studies (32,33,36) are summarised in Table 1.2. From these studies, it appears that C6 ceramide loading should be kept below 30 mol% to avoid interfering with vesicle stability (32,40). Importantly, such high loading have only been achieved by including PEG(750)-C8 ceramide in the formulation (32). Unfortunately, to date, there is not enough information regarding the impact of composition

and size of liposome on ceramide delivery, thus more work is needed to investigate these matters.

Still, liposomes have several drawbacks as a drug carrier, including premature release or leakage of lipophilic contents and relatively low loading capacity for hydrophobic substances compared to other lipid-based nanoparticles (63–67). This suggests that nanoparticles other than liposomes may be more effective delivery system for C6 ceramide and that more work is needed to confirm this. For instance, PLGA (poly-lactic-co-glycolide)/ liposome hybrids for ceramide delivery revealed an extended release of ceramide compared to the liposomes without PLGA, where ceramide completely released in 2 minutes (68). Moreover, Wang *et al.* (69) found that C6 ceramide-loaded graphene oxide-polyethylene glycol-polyethylenimine nanoparticles (NGO-PEG-PEI/C6) considerably increased the activation of caspase-3 that indicate apoptosis in hepatocellular carcinoma cells (HepG2), compared to liposome-C6 ceramide and the vehicle control used (70).

To date, few drug carriers have been explored for the encapsulation of C6 ceramide. Although liposomes are a relatively common example, solvent-free lipid nanocapsules (LNCs) can offer a new platform for ceramide delivery (71).

1.4. Lipid nanocapsules (LNCs)

Lipid nanocapsules (LNCs) are nano-emulsions characterised by a liquid oily core and a mixture of surfactant and phospholipids as the semi-solid outer shell. For most LNCs, the oily core consist of medium-chain triglycerides while the shell is formed by a combination of polyethylene glycol hydroxystrearate (HS-PEG) and soybean lecithin (Figure 1.3). Compared to liposomes, LNCs have several advantages, including a robust, solvent-free

manufacturing process, narrow size distribution, and high encapsulation efficiency for hydrophobic drugs (71,72).

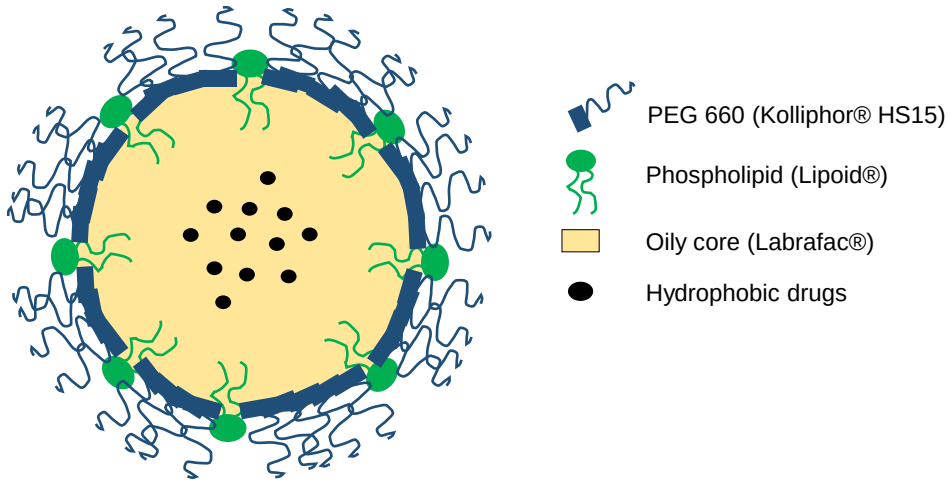

Figure 1.3. Schematic representation of LNCs structure; adapted from (71) with modification and permission from Elsevier.

LNCs are prepared using a phase-inversion temperature method, developed and patented by Heurtault *et al*. (pub no. US 2009/0238865 A1). This method involved three cycles of a heating-cooling process followed by dilution with cold water to induce an irreversible shock from water-in-oil (w/o) to oil-in-water (o/w) emulsions (71,73). A ternary diagram was plotted to determine the optimal proportions of each component required to form LNCs. This revealed that LNCs are formed within the following limits: 10 – 40% of hydrophilic surfactant (HLB: 14 – 16), 10 – 25% of oil, and 35 – 80% of water (73,74). As expected, LNC size decreased with surfactant concentration and increase with oil content (71,73–75).

LNCs rely on the addition of Kolliphor® HS15 which contains HS-PEG, to create a stable nanocarrier with prolonged circulation times (76,77). Kolliphor® HS15 is a FDA-approved PEGylated derivative of stearic acid (C18) (Figure 1.4). Interestingly, HS-PEG in the LNCs has been found to inhibit the P-glycoprotein (P-gp) efflux pump that contributes

to the multidrug resistance (MDR) in cancer cells (78,79). It should be noted, however, that the presence of excess free surfactant chains may lead to toxicity when unpurified LNCs are tested on cells (74,80). Indeed, the amphipathic nature of the surfactant allows it to disrupt cell membranes (80,81). The same mechanism can lead to haemolysis of red blood cells (82). However, Kolliphor® HS15 showed a lower haemolytic activity than polysorbate 80, a common pharmaceutical excipient, and no haemolytic if used at low concentrations (≤ 1%) (83–85). Therefore, purification will be paramount to control levels of free surfactant in LNC formulations.

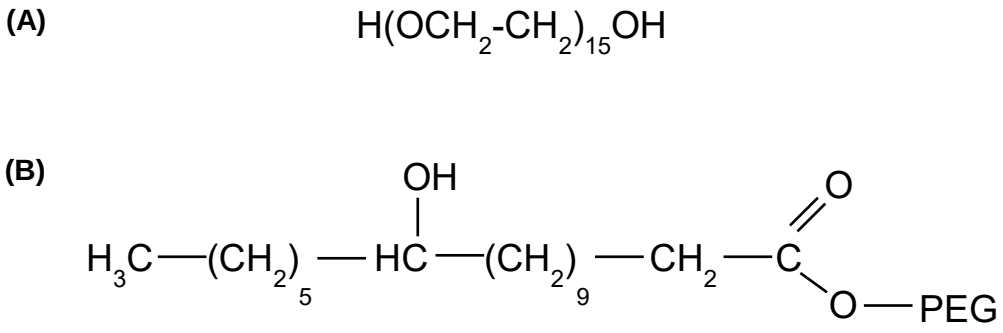

Figure 1.4. Chemical structure of (A) PEG 660 and (B) PEG 660-HS found in Kolliphor® HS15; adapted from (77) with permission from Wiley.

Recently, research on the application of LNCs as nanocarriers for anticancer drug delivery has increased (86–90). LNCs have shown a higher capacity for poorly-soluble, non-ionisable drugs such as paclitaxel and docetaxel, compared to liposomes (71,78). Similar entrapment efficiencies are expected for short-chain ceramide. This combined with the potential inhibition of the P-gp by HS-PEG could allow LNCs to dramatically boost the activity of chemotherapeutic agents (31,91).

Furthermore, although nano-emulsions or solid lipid nanoparticles have been explored for C6 ceramide delivery (92–95), it remains unclear whether those carriers address the issues raised about liposomes since no direct comparison was provided. Moreover, the specific use of LNCs for ceramide delivery has not been studied yet. Therefore, here, LNCs are selected as a potential alternative to liposome for C6 ceramide delivery against breast cancer cells because of their promising characteristics.

1.5. Aim and objectives

This research project was designed to determine whether LNCs could be a suitable alternative nanocarrier for C6 ceramide as a bioactive, pro-apoptotic sphingolipid. It is hypothesised that LNCs will be a suitable alternative to liposome as nanocarriers for ceramide delivery to MDA-MB-231 breast cancer cells.

Objectives:

1. Manufacture and characterisation of LNCs with and without C6 ceramide using a phase-inversion temperature method.
2. Manufacture and characterisation of PEGylated liposomes with and without C6 ceramide using a thin film hydration method.
3. Assess the impact of C6 ceramide on cytotoxicity of LNCs and liposome against MDA-MB-231 cell line using Cell-Counting Kit 8 (CCK8) method.
4. Study the impact of encapsulation on cytotoxicity of C6 ceramide towards MDA-MB-231 cell line using analysis of variance (ANOVA).
5. Probe the mechanism of cell death induced by C6 ceramide using annexin V/ PI and caspase-3/7 assay.

2. Nanoparticles manufacturing and characterisation

2.1. Introduction

Characterisation of a nanoparticle's physico-chemical properties is an essential step following their preparation. Typically, properties such as average diameter, size distribution (polydispersity index), surface charge (zeta potential) and sometimes morphology are assessed. Understanding these properties is beneficial to help predict the behaviour of the nanoparticles in the body (96,97). For example, the size and surface properties of nanoparticles determines their circulation times in the bloodstream and rapid clearance by the mononuclear phagocyte system (MPS) (98,99). Smaller, hydrophilic, neutral particles tend to have longer circulation times, while larger, cationic, hydrophobic nanoparticles could be recognised by MPS and, on occasion, induce an inflammatory response (100,101).

Dynamic light scattering (DLS) is one of the most popular techniques to determine hydrodynamic particle size. DLS measures fluctuations in the intensity of light scattered by suspended nanoparticles subject to Brownian motion and provides a simple and rapid measurement method (102,103). DLS also estimates the particle size distribution data which is displayed as polydispersity index (PdI) (103,104). PdI values <0.3 are considered acceptable and indicate a homogenous nanoparticle population (105).

Furthermore, surface properties, such as surface charge and hydrophobicity, also influence the interaction between nanoparticle and biological systems. Zeta potential (ZP) is linked to surface charge and is determined based on electrophoretic mobility and can be used to predict the colloidal stability of nanoparticles (106). According to the DLVO theory on the stability of colloid, a near-neutral ZP (- 25 mV< ZP< 25 mV), is associate with a higher risk of nanoparticle aggregation due to the interparticle interaction (e.g. van der Waals, electrostatic). For these particles, steric stabilisation with a hydrophilic coating may be

needed to maintain stability. On the other hand, charged particles (ZP greater or lower than ± 60 mV) have an excellent stability (103,107). Yet, strongly positive particles may be more toxic and may have limited stability under physiological conditions (108–112).

In addition to the surface charge, the hydrophobicity of nanoparticle is another key property, though not routinely assessed, that determines the fate and bioavailability of nanoparticles (113,114). Hydrophobic nanoparticles can aggregate at physiological salt concentrations due to a salting-out effect (115,116). Surface hydrophobicity also influence the cellular uptake and toxicity of nanoparticles as drug carriers (113,117–119), and has been associated with the 'protein corona' which can affect the distribution and transport of nanoparticles in physiological and environmental systems (120–122). Numerous techniques have been suggested to evaluate surface hydrophobicity, either quanti- or quali-tatively: salt aggregation, probe adsorption method, contact angle, and hydrophobic interaction chromatography (HIC) (113,117,123). Salt aggregation test (SAT) will be used in this current study to determine the hydrophobicity property of nanoparticles based on a salting-out phenomenon (124).

2.1.1. Aim and objectives

This chapter will focus on the manufacture and basic characterisation of LNCs and liposome with and without C6 ceramide. The results obtained will be analysed to test the research hypothesis that the presence of C6 ceramide will not have a major impact on the physico-chemical properties and surface hydrophobicity of nanoparticles.

Objectives:

1. Manufacture LNCs and liposome with and without C6 ceramide and assess their particle size (DLS), size distribution (DLS), zeta potential (electrophoretic mobility), including as part of a colloidal stability study.

2. Assess surface hydrophobicity using the salt aggregation test method.

2.2. Materials and methods

2.2.1. Materials

Kolliphor® HS15 (PEG660-C18; 30% free PEG 660 and 70% PEG 660 hydroxystearate) and Labrafac™ Lipophile WL 1349 (medium-chain triglyceride (MCT): caprylic [C8] and capric [C10] acids) were kindly provided by BASF SE (Ludwigshafen, Germany) and Gattefosse (Saint-Priest, France), respectively. Lipoid® S75 (SPC; soybean phospholipid with 70% phosphatidylcholine), DSPC (1,2-Distearoyl-sn-glycero-3-phosphocholine) and PEG (2000)-DSPE (N-(Carbonyl-methoxypolyethyleneglycol-2000)-1,2-distearoyl-sn-glycero-3-phosphoethanolamine) were purchased from Lipoid GMBH (Ludwigshafen, Germany). Sodium chloride (NaCl), ammonium thiocyanate (NH_4SCN) and cholesterol were purchased from Merck (Gillingham, Dorset, UK). Ferric chloride anhydrous ($FeCl_3$) from Scientific Laboratory Supplies Ltd. (Wilford, Nottingham, UK) and chloroform from Thermo Fisher Scientific Ltd. (Loughborough, Leicestershire, UK). C6 Ceramide (d18:1/6:0) was purchased from Cambridge Bioscience Ltd. (Cambridge, UK).

2.2.2. Methods

2.2.2.1. Preparation and purification of LNCs

LNCs were prepared using the phase-inversion method previously described by Hertault *et al*. (73). Briefly, a mixture of Lipoid® S75, Kolliphor® HS15, Labrafac™ Lipophile WL1349 and 3% NaCl aqueous were mixed and heated to 85ºC under constant stirring. Two sizes of LNCs were prepared by varying composition according

to Table 2.1. The coarse emulsion was then subjected to three cycles of heating-cooling (85ºC – 60ºC – 85ºC – 60ºC – 85ºC). When the mixture reached 72ºC during the last cooling step, cold water (2 – 4ºC) was poured into the mixture, leading to the spontaneous formation of stable LNCs. The LNC dispersions were stirred for 5 minutes at room temperature. The amount of cold water added to the mixture was 2.5-times and 2-times the total weight of the original emulsion for LNC50 and LNC100, respectively. LNC concentration was estimated from the oil content from the initial formulation with 34.29 mg/mL and 76.67 mg/mL for LNC50 and LNC100, respectively. LNC emulsions were stored at 4ºC until further use and were stable for at least 8 weeks at that temperature. C6 ceramide-containing LNCs were prepared using the protocol above with the amount of ceramide listed in Table 2.1.

Table 2.1. LNCs composition

Formula	Composition (% w/w)				
	Labrafac® Lipophile WL1349	**Kolliphor® HS15**	**Lipoid® S75**	**$NaCl_{aq}$ 3%**	**C6 Ceramide**
LNC50-ghost	12	10.5	1.5	76	-
LNC50-C6	12	10.5	1.5	76	0.05
LNC100-ghost	23	8.5	1.5	67	-
LNC100-C6	23	8.5	1.5	67	0.09

The excess surfactant and free PEG660 (Kolliphor® HS15) were removed by dialysis (Float-A-Lyzer® G2, UK; 1000 kD MWCO) against 2L of deionized water containing 4 g of BioBeads® SM-2. The water was changed daily during the purification process for 7 days. Residual surfactant was determined colorimetrically (117) by separating the excess surfactant from the particle using ultrafiltration (Amicon Ultra;

100 kDa MWCO; Milipore, UK, 11,357 x *g* for 10 minutes). For this step, 50 µL of ultrafiltrate supernatant containing Kolliphor® HS15 was added to the mixture of 750 µL of chloroform and 750 µL of aqueous solution of ammonium ferrothiocyanate (16.2 g/L $FeCl_3$; 30.4 g/L NH_4SCN). The biphasic mixture was incubated under gentle orbital stirring for 30 minutes at room temperature in the dark. The bottom chloroform layer was collected and measured the absorbance using UV-Vis spectrophotometer (Shimadzu UV-2600; Kyoto, Japan) at wavelength 510 nm (Shimadzu UV-2600; Kyoto, Japan). Validation of the assay methods based on three individual batches of surfactant revealed a linear range 0.5 – 4 mg/mL, a limit of detection (LoD) 0.21 mg/mL, and a limit of quantification (LoQ) 0.63 mg/mL. The surfactant content determined from a calibration curve ($y = 0.1538\ x + 0.0753$; $R^2 = 0.9977$).

2.2.2.2. Preparation of liposomes

Liposomes were prepared using the thin-film hydration method. Briefly, DSPC, cholesterol, PEG (2000)-DSPE and C6 ceramide were combined in specific molar ratios (Table 2.2) and dissolved in chloroform. The solvent was removed by rotary evaporator at 55°C for 60 mins to form a lipid film. The lipid film was then hydrated by the addition of 0.9% NaCl to obtain a final lipid concentration of 10 mg/mL. The dispersion was sonicated at 60°C for 5 – 10 minutes and then manually extruded at 60ºC through 100 nm polycarbonate membranes (Avanti Mini-Extruder, Avanti Polar Lipids, Alabaster, Alabama, USA). Liposomes were stored at 4ºC until further use.

Table 2.2. Liposomes composition

Formula	Composition (mol%)			
	DSPC	**Cholesterol**	**PEG (2000)-DSPE**	**C6 ceramide**
Liposome-Ghost	56.6	28.7	14.7	-
Liposome-C6 Ceramide	55	22.5	7.5	15

2.2.2.3. Size and surface charge measurement

Particle size, polydispersity index (PdI), and zeta potential (ZP) of nanoparticles were measured on a Zetasizer® Malvern Nano series (Malvern Nano-ZS, Malvern, UK). The measurements were carried out at temperature 25ºC and scattering angle 173º. Refractive index for all samples was set at 1.590. The PdI was used to estimate the size distribution with a PdI value less than 0.3 indicates a unimodal size distribution. Prior to measurement, both the LNCs and liposomes were diluted 1:20 in deionized water and 10 mM NaCl for size and zeta potential measurement, respectively.

2.2.2.4. Stability study of nanoparticles

The colloidal stability of nanoparticles was assessed under storage (4ºC) and cell culture conditions (sterile cell culture media (Dulbecco's Modified Eagle Medium high glucose containing 10% foetal bovine serum (FBS) and 5% penicillin-streptomycin) and incubated under sterile condition at 37ºC). In both cases, particle size and PdI were measured daily for 10 days. For cell culture conditions, the measurement settings were adjusted at temperature 37ºC, viscosity 0.7400 cP and refractive index 1.337.

2.2.2.5. Assessment of nanoparticle surface hydrophobicity

This experiment was conducted using a salt aggregation test (SAT). Briefly, LNCs and liposomes were diluted in saline solutions at various NaCl concentration (2.5 M to 5 M) and at two different temperatures, 25ºC and 37ºC. Aggregation was observed by measuring the change in particle size over 30 minutes. Settings were adjusted to mimic the changes in refractive index and viscosity of the dispersing medium at increasing salt concentration.

2.2.2.6. Statistical analysis

Graph processing and statistical analyses were performed using GraphPad Prism version 9 (GraphPad Software Inc.,California, USA). Properties of LNCs and liposomes were analysed using an unpaired t-test. Results from the stability study for ceramide-loaded liposomes were analysed using one-way ANOVA with time as the sole variable, followed by a post-hoc Dunnett test. Salt aggregation test statistical analysis was performed using a two-way ANOVA with time and salt concentrations as variables and post hoc Dunnett's test for multiple comparisons.

2.3. Results and discussion

2.3.1. Manufacture and characterisation of LNCs

In this study, LNCs were successfully prepared using the phase-inversion temperature method previously reported (73). As expected, LNC size could be controlled by varying the oil (Labrafac® Lipophile WL 1349) and surfactant (Kolliphor® HS15) content, according to the ternary diagram proposed by Hertault *et al*. (73). In this study, two different sizes of LNCs were prepared (50 nm and 100 nm). In both cases, the

diameters obtained by DLS agreed with the predicted sizes. Furthermore, introduction of C6 ceramide had no noticeable impact on particle size, polydispersity index. This was somewhat expected as the ceramide loading was relatively low. Since C6 ceramide is a natural cellular sphingolipid with a short hydrophobic region, it was originally predicted that the ceramides would be inserted at the capsule interface like the phospholipid in the LNCs (Figure 2.1). However, it remains possible for some or all the C6 ceramide to be dissolved in the oily core as well, especially as it was found that up to 1 mg/mL C6 ceramide could be dissolved in Labrafac. The activity of C6 ceramide formulated as LNCs systems will be the focus of chapter 3.

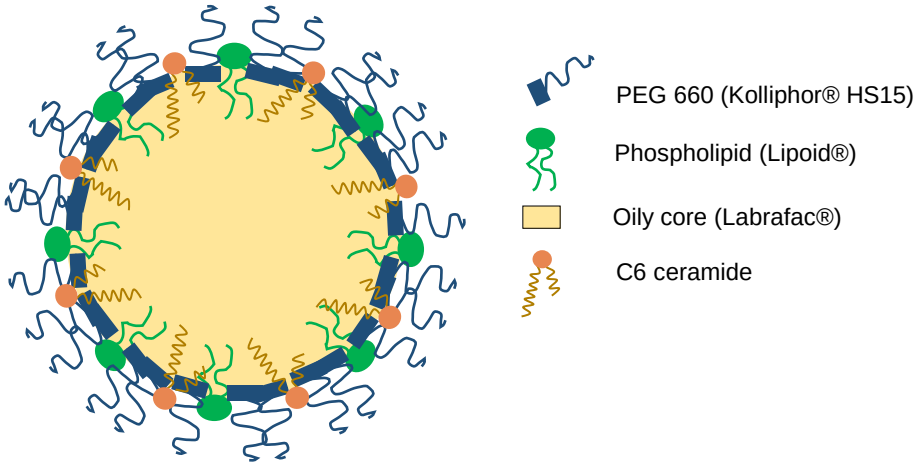

Figure 2.1. Schematic representation of LNC-C6 structure.

After preparation, the LNCs (with and without ceramide) were purified to remove the excess surfactant which has been associated to cytotoxicity (80,81). In a previous study, Vonarbourg *et al.* (77) showed a 30% decrease in the concentration of free surfactant after 48 hours of dialysis using a 50 kDa MWCO membrane, against deionised water. It was predicted that the removal of excess surfactant could be achieved optimally with a higher molecular cut-off.

Here, optimisation using surfactant stock solution (10 mg/mL) has been carried out to obtain appropriate conditions for LNCs purification. At this concentration, the surfactant is expected to exist in a mixture of free chains and micelles. However, even when using a dialysis membrane with a cut-off (1,000 kDa) 20 times higher than the molecular weight of surfactant chains, only a small amount of surfactant was removed after 3 days of purification against deionised water (data not shown). This may reflect the difficulty in removing surfactant micelles from the preparation as the cut-off is less than 10-fold the reported MW of Kolliphor micelle (163 kDa) (83). Therefore, the addition of modified resin adsorbent (BioBeads® SM-2 Resin) was needed to encourage surfactant removal.

Based on a previous study conducted by Jones *et al*. (117), the inclusion of adsorbent during LNC dialysis accelerated purification and led to the decrease of free surfactant concentrations to <0.5 mg/mL in 72 hours. Nonetheless, in the current study a longer duration (168 hours) was required to achieve similar results and produced surfactant concentrations lower than the limit of quantification (LoQ: 0.63 mg/mL). The correlation between the concentration of surfactant and the toxicity will be discussed in chapter 3.

The properties of ghost and ceramide-loaded LNCs before and after purification are summarised in Tables 2.3 – 2.4. After purification, a slight, but statistically significant, increase in average size was noted for LNC100s only, however, that size remained within acceptable variation for nanoparticles. More interestingly, the PdI increased dramatically for both ghost LNCs after purification, though values remained within the acceptable range (PdI < 0.3). The exact reasons behind these observations are unclear, especially as these occurred without a notable change in particle size. However, the increase in PdI

might be correlated to the rearrangement of PEG chains during dialysis (77). Importantly, although the PdI increased after purification, no further increases were noted over time, confirming adequate colloidal stability.

Table 2.3. Properties of LNCs-ghost before and after purification

Parameter	Before Purification		After Purification	
	LNC50-ghost	**LNC100-ghost**	**LNC50-ghost**	**LNC100-ghost**
Average diameter (nm)	48 ± 3	100 ± 4	47 ± 3	112 ± 2***
PdI***	0.07 ± 0.07	0.06 ± 0.02	0.22 ± 0.05	0.23 ± 0.02
Zeta potential (mV)	-7 ± 2	-6 ± 1	-6 ± 1	-7 ± 1
Theoretical surfactant concentration (mg/mL)	30.00	28.33	-	-
Actual surfactant concentration (mg/mL)	32.48	29.59	<LoQ	<LoQ

(1)Data are presented as mean ± SD from three individual batches (*n*=3)
(2)Statistical analysis was performed, using an unpaired t-test to compare individual LNC formulations before and after purification (****p<0.001* pre- vs post-purification).

Similarly, an increase in PdI was noticed for both C6 ceramide-loaded LNCs after dialysis. Furthermore, LNCs were found to have a neutral to slightly negative zeta potential, like in previous studies (125,126). This parameter was not affected by purification as no statistical difference was observed for any of the formulations (*p>0.05*).

Table 2.4. Properties of LNCs-C6 before and after purification

Parameter	Before Purification		After Purification	
	LNC50-C6	**LNC100-C6**	**LNC50-C6**	**LNC100-C6**
Average diameter (nm)	44 ± 1	100 ± 1	47 ± 2	112 ± 5***
PdI***	0.04 ± 0.01	0.07 ± 0.03	0.24 ± 0.02	0.19 ± 0.07
Zeta potential (mV)	-6 ± 3	-7 ± 2	-8 ± 4	-8 ± 1

(1)Data are presented as mean ± SD from three individual batches (*n*=3)
(2)Statistical analysis was performed, using an unpaired t-test to compare individual LNC formulations before and after purification (****p<0.001* pre- vs post-purification).

A stability study was also conducted on purified ghost and C6-loaded LNCs under storage (4°C) and cell culture conditions. All LNCs formulations were stable when stored in the fridge (Figure 2.2) which agrees with previous findings showing that LNCs are stable at this temperature for up to 18 months (73).

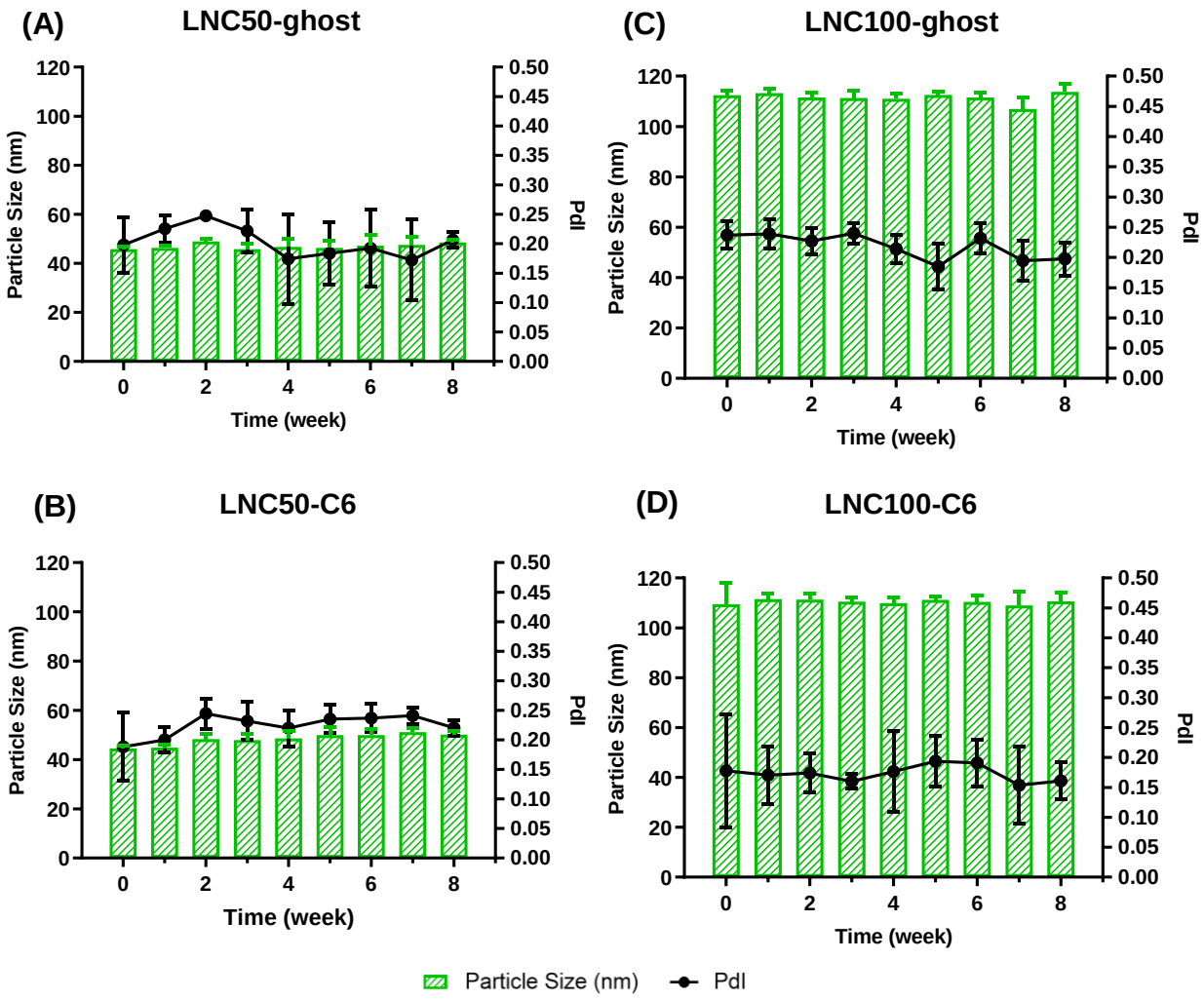

Figure 2.2. Stability study of LNCs with and without ceramide under storage at 4°C with (A,B) LNC50; (C,D) LNC100. Data presented as mean ± SD from three individual batches (*n*=3).

In addition, although the colloidal stability at room temperature was not tested here, previous studies reported that LNCs were stable at room temperature (25°C) and even at higher temperatures (37° – 40°C) for 1.5 months, and there is no indication this would

not be the case for the LNCs prepared here (73,117,127). The steric stabilisation provided by the PEG and the semi-rigid shell led to the physical stability of LNCs and prevented the coalescence of the oil core (74).

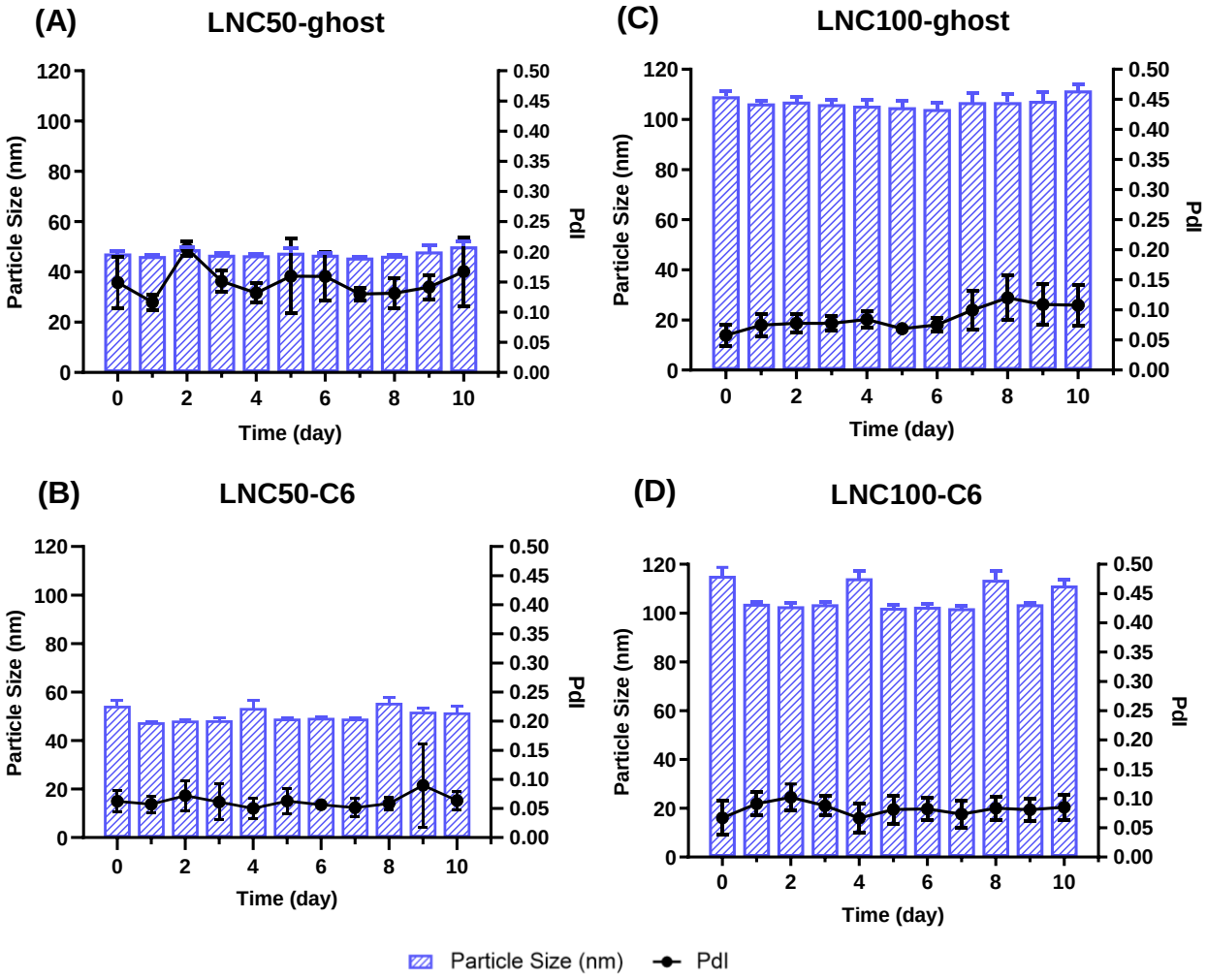

Figure 2.3. Stability study of LNCs with and without ceramide under cell culture conditions with (A,B) LNC50; (C,D) LNC100. Data presented as mean ± SD from three individual batches (*n*=3).

The stability under cell culture conditions aimed to mimic *in vitro* conditions by dispersing the nanoparticles in complete cell culture media. Both LNC50s and LNC100s with and without C6 ceramide were relatively stable for 10 days, which is more than required for most cell assays (Figure 2.3). There was a slight change of particle size and

PdI of LNCs during the study period, but PdI remained within the acceptable range (PdI < 0.3) and particle size was within 5 – 10 nm of the initial value.

Overall, LNCs with and without C6 ceramide were successfully prepared with the phase-inversion temperature method with good physico-chemical properties and stability. The addition of bioactive sphingolipid, C6 ceramide, did not dramatically influence the characteristics and stability of LNCs formulations.

2.3.2. Manufacture and characterisation of liposomes

Control DSPC liposome formulations were prepared by thin-film hydration. DSPC is a fully saturated neutral C18-phospholipid with a phase transition temperature ca. 55ºC, that has been shown to enhance liposome stability (128,129). In addition, DSPC has a rigid cylindrical structure (130) and produces fairly thick lipid bilayers (44.30 ± 0.11 Å) (131) which produces spherical liposome and could enhance encapsulation efficiency of hydrophobic substances, compared to unsaturated phospholipid with a similar chain length or other phospholipids with shorter alkyl chains (130,132).

The properties of liposomes with and without C6 ceramide are summarised in Table 2.5. There was a significant difference in size between liposome-ghost and liposome-C6, with the latter showing larger particle size, as expected. PdI remained low (<0.3), even after C6 loading. The zeta potential for both liposomes was found to be slightly negative to neutral which as previous reported by Overbye, *et al.* (49) and Zolnik, *et al.* (133).

Table 2.5. Properties of liposome with and without C6 ceramide

Parameter	Liposome-Ghost	Liposome-C6 ceramide
Average diameter (nm)	68 ± 1	91 ± 2***
PdI	0.16 ± 0.01	0.19 ± 0.02
Zeta potential (mV)	-8 ± 2	-9 ± 1
Lipid concentration (mg/mL)	10	10

(1)Data are presented as mean ± SD from three individual batches (n=3)
(2)Statistical analysis was performed using unpaired t-test ($^{***}p<0.001$ liposome-ghost vs liposome-C6)

Chemical and colloidal stability of liposomes during storage and under cell culture conditions can be affected by their composition. Here, the use of DSPC and addition of cholesterol are expected to circumvent some of those issues (130,134). Cholesterol improves vesicle stability by regulating the fluidity of lipid bilayer (135,136). Furthermore, the addition of PEG in liposome formulations, especially with C6 ceramide-loaded, is expected to provide steric stabilisation and prevent liposome aggregation over time (128,137). PEG (2000)-DSPE is a polar lipopolymer with large headgroups and adopts a truncated cone-shaped structure that can fit into the gaps between phospholipid (cylinder-shaped) and cholesterol (inverted truncated cone-shaped) or short-chain ceramides (inverted truncated cone-shaped), thus further stabilising the liposomal bilayer (Figure 2.4) (45,138).

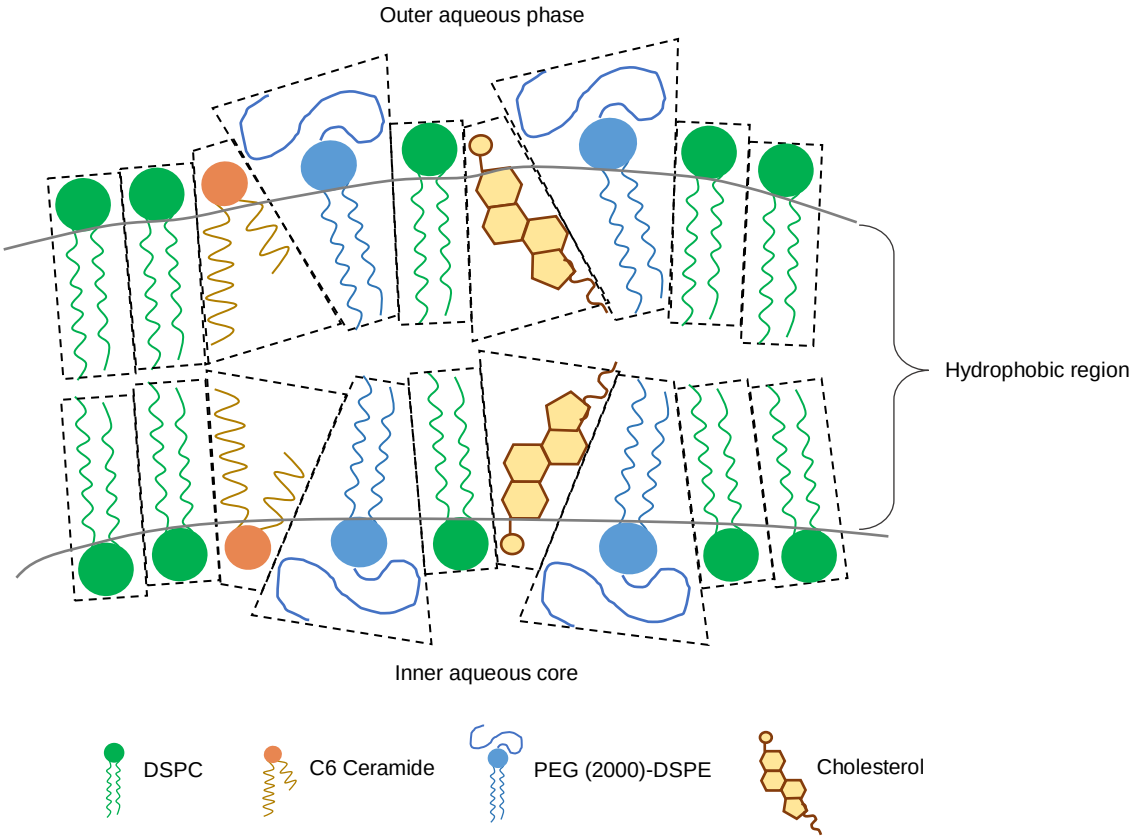

Figure 2.4. Schematic illustration of space-filling models of bilayer formed from DSPC, cholesterol, PEG (2000)-DSPE and C6 ceramide; adapted from (45) with modification and permission from American Chemical Society.

Despite the presence of PEG and cholesterol, there was a noticeable difference in terms of stability between liposome-ghost and liposome-C6 (Figure 2.5). Ghost liposomes were relatively stable both under storage conditions (at 4°C) and in cell culture media, during the study period. Though a small change was observed in terms of particle size and size distribution, it was not that remarkably different from the initial value. In contrast, C6 ceramide-loaded liposome showed poorer colloidal stability than ghost liposome, with evidence of aggregation taking place from day 13 (4°C) and day 9 (cell culture conditions). Interestingly, the difference in stability between ghost and C6 liposomes was less striking under cell culture conditions. This phenomenon demonstrates

that the presence of C6 ceramide in liposome formulation markedly influences the stability of lipid bilayer systems with the same preparation method as ghost liposome.

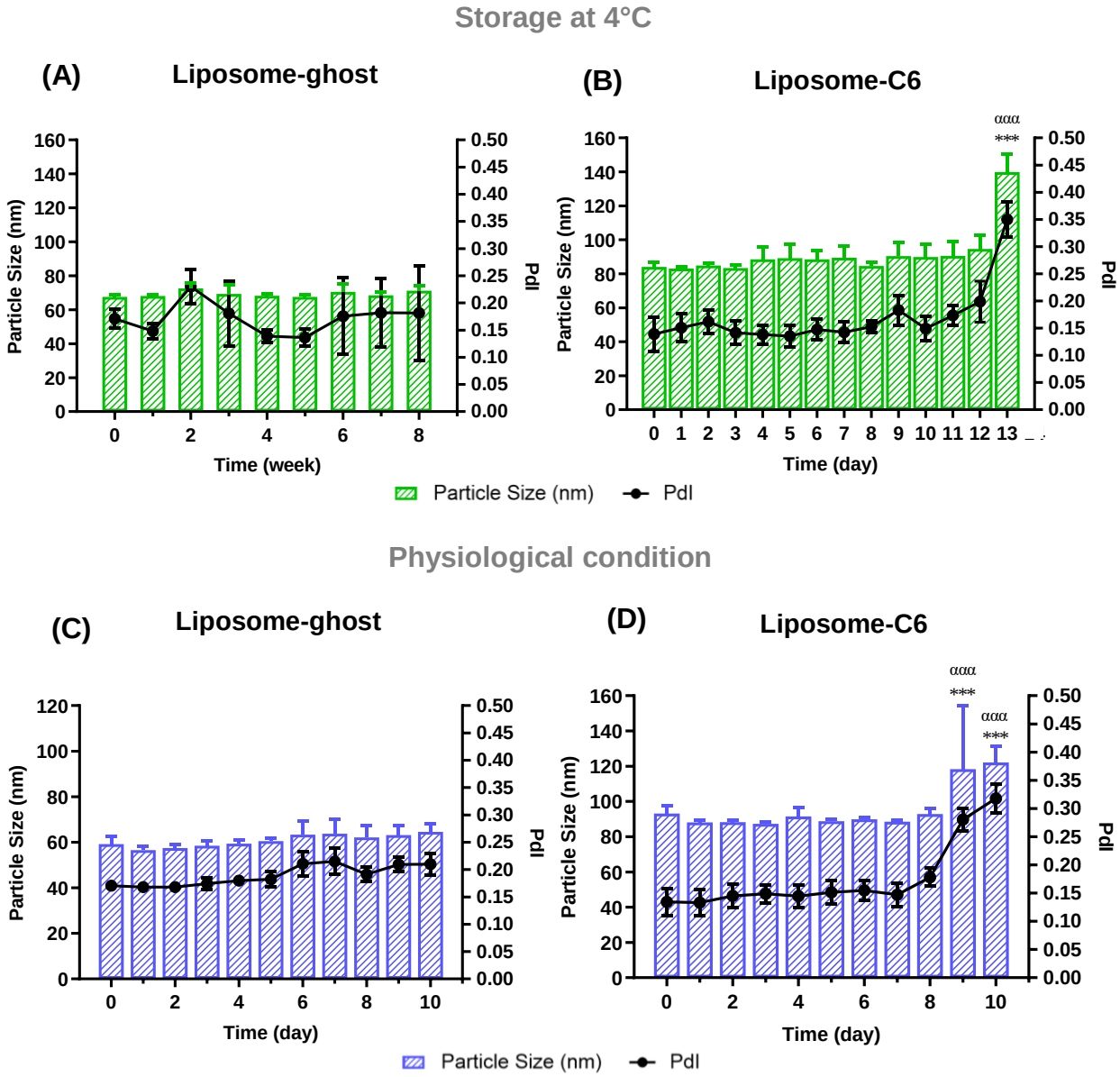

Figure 2.5. Stability study of liposome formulations under storage at 4°C and cell culture conditions with (A,C) liposome-ghost; (B,D) liposome-C6. Data presented as mean ± SD from three individual batches (n=3). Statistical analysis using one-way ANOVA followed by a post-hoc Dunnett test for particle size ($^{***}p<0.001$) and PdI ($^{\alpha\alpha\alpha}p<0.001$), compared to the initial measurement at week/day 0.

The composition of lipids seems to affect the stability of liposome-C6 ceramide. Here, it is possible that the organisation and stability of the liposome bilayer was affected by the addition of C6 ceramide, an unsaturated sphingolipid. (139,140). Moreover, the PEG content in ceramide liposomes (7.5 mol%) was less than in ghost liposomes (14.7 mol%), which potentially reduced colloidal stability overtime.

To conclude, liposome formulations with good characteristics were successfully manufactured. The presence of C6 ceramide seems to affect the physico-chemical properties and stability of liposomes. The stability parameter may be correlated to the surface hydrophobicity of nanoparticles which will be discussed in the next section.

2.3.3. Assessment of nanoparticle surface hydrophobicity

Surface hydrophobicity is an essential property that influences the stability and biodistribution of nanocarriers (121). In this study, salt aggregation test (SAT) which based on the salting-out of hydrophobic colloids at high ionic strength was used to assess this characteristic. It is important to note that the salt concentrations used are considerably higher than physiological concentrations. The SAT test assesses hydrophobicity based on the extent of aggregation and the minimum NaCl concentration triggering aggregation. Although this method provides a rapid and simple qualitative assessment, it has several limitations including low specificity on particle-ion interaction, dependence on nanoparticle concentration and lack of standardized protocols (141,142).

Theoretically, nanoparticles with high surface hydrophobicity will be more likely to aggregate when exposed to concentrated salt solution at 37°C (143). For LNCs, it was projected that LNC100s with higher oil content and lower surfactant concentrations

would be slightly more hydrophobic compared to the LNC50s. However, the results indicated the opposite.

At room temperature (25ºC), no aggregation was observed for any of the LNCs, with and without ceramide. Still, LNC50-ghost, LNC50-C6 and LNC100-C6 all showed a slight increase in particle size (ca. 1.5-fold) when exposed to high salt concentration (5M). On the other hand, the aggregation was observed for both ghost and C6-loaded LNC50s when incubated in 2.5 M $NaCl_{aq}$ at 37ºC (Figure 2.6 B and D), with diameter increasing ca. 3-fold. Further increases in NaCl concentrations led to ca. 10-fold and 35-fold increase in particle sizes at 4 M and 5 M NaCl solutions 37ºC, respectively. LNC100 preparations (Figure 2.7) also experienced an increase in size, though to a lower extent ca. 5-fold and 10-fold for 4 M and 5 M NaCl solutions 37ºC, respectively. However, the presence of C6 ceramide did not affect the surface behaviour of LNCs.

Salting-out is more likely to occur at higher temperatures when the interaction between ion and water becomes stronger (124). Salting-out depends on the hydrophobicity of the particles and particles with minimum exposed hydrophobic zones tend to remain fully dispersed even at high salt concentrations (124,144).

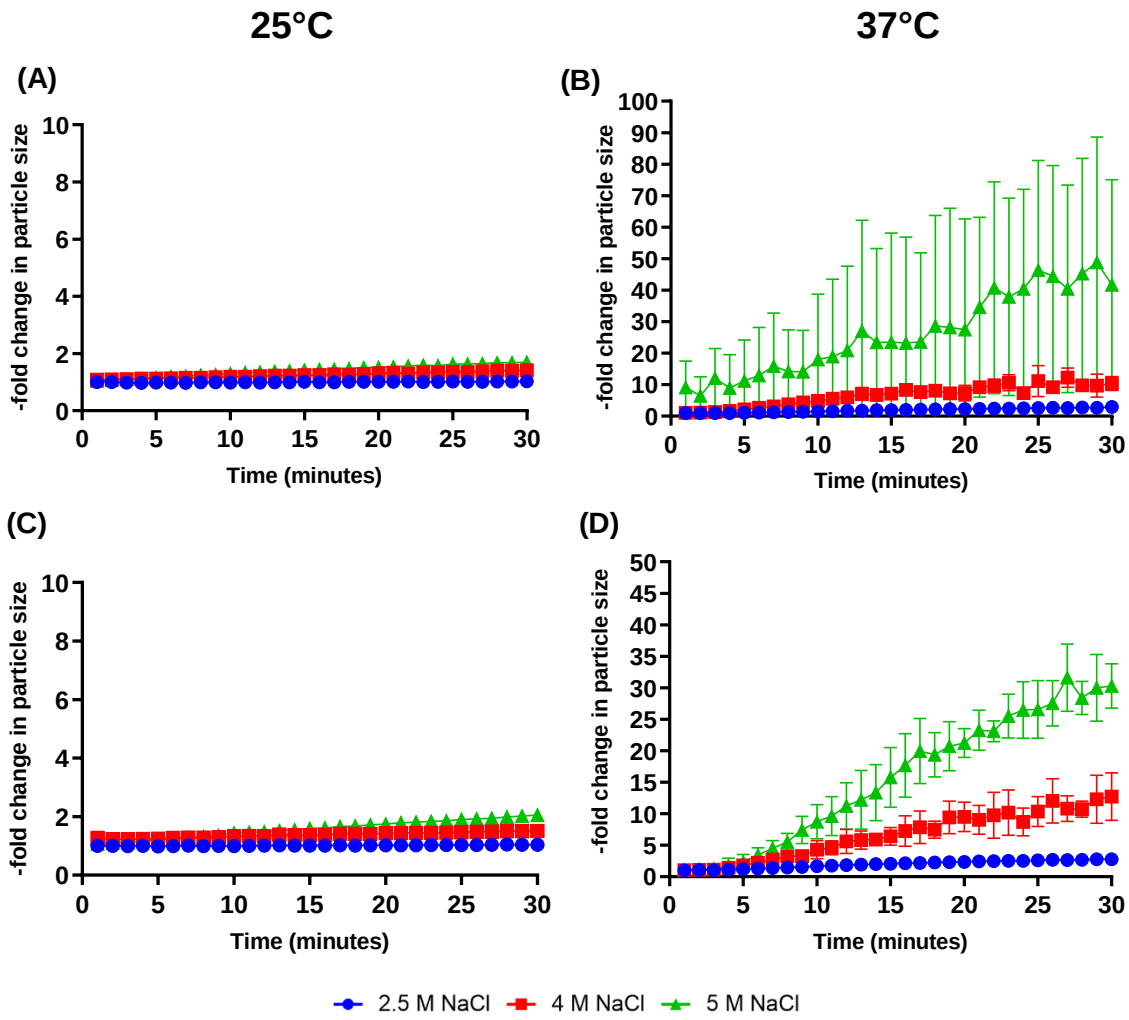

Figure 2.6. Salt aggregation test of LNC50 at 25° and 37°C with (A,B) LNC50-ghost; (C,D) LNC50-C6. Data presented as mean ± SD from three individual batches (*n*=3). Statistical analysis using two-way ANOVA followed by a post-hoc Dunnett test, compared to the initial measurement at minute 0.

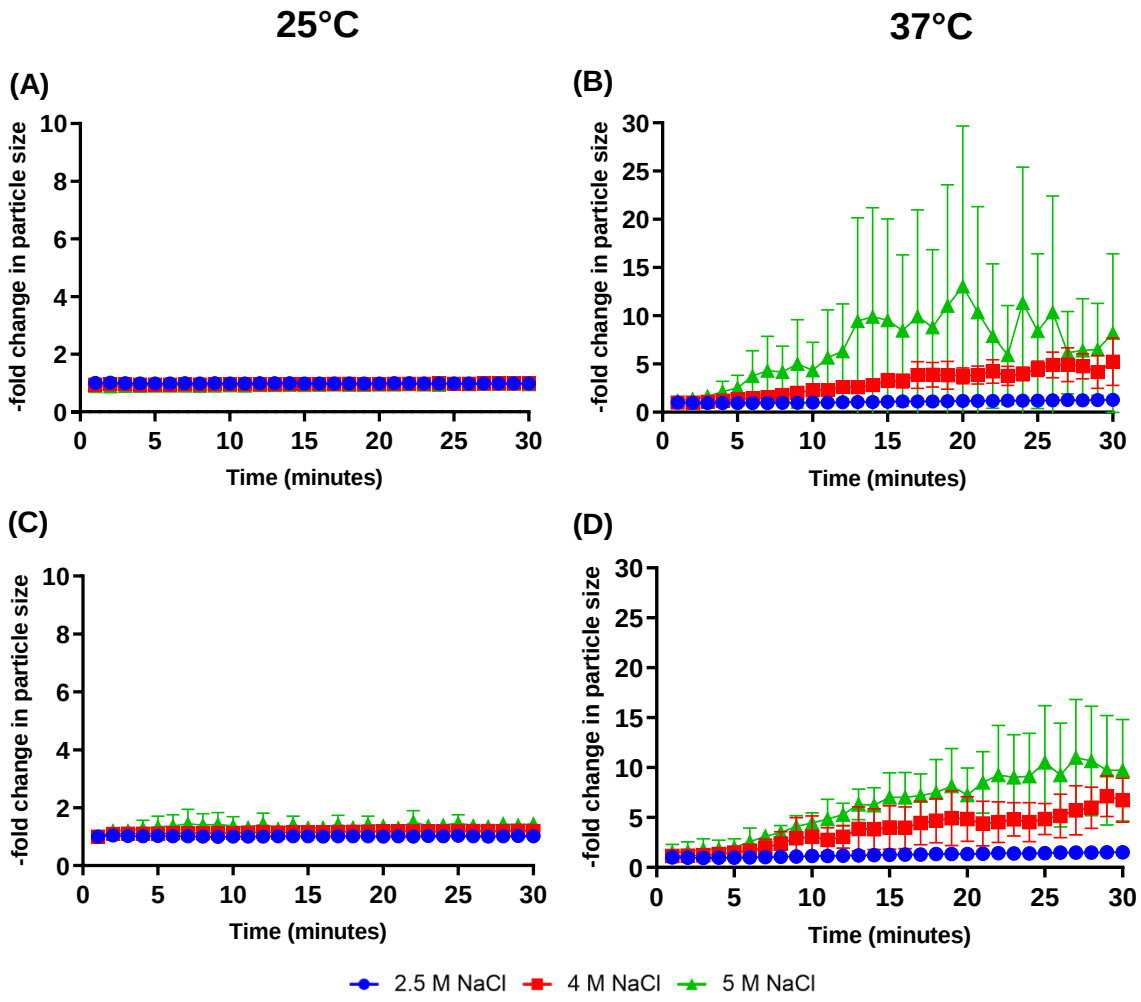

Figure 2.7. Salt aggregation test of LNC100 at 25° and 37°C with (A,B) LNC100-ghost; (C,D) LNC100-C6. Data presented as mean ± SD from three individual batches (*n*=3). Statistical analysis using two-way ANOVA followed by a post-hoc Dunnett test, compared to the initial measurement at minute 0.

It was observed that aggregation for both LNC sizes was salt concentration- and time-dependent, with LNC50 formulations appearing to be more hydrophobic than LNC100. This unexpected outcome could be explained by differences in the conformation of PEG chains on the surface of the LNCs. Numerous studies have suggested that PEG can exist in one of two conformations: brush or mushroom, with the later more suited to steric stabilisation. The conformation adopted by PEG will depend on particle size and PEG content with lower densities, more likely to be in a mushroom

conformation, while higher densities will exist in the more rigid brush conformation (145,146). Here, the combination of a lower density and lower curvature mean that PEG is more likely to adopt a mushroom conformation on LNC100s and have the flexibility to interact with water, leading better hydration and better protection against aggregation when exposed to salt solutions. It has also been suggested that the conformation of the PEG can affect the interaction with ions present in the dispersing medium. Indeed, a previous study confirmed that ions could penetrate deeper into the corona of LNC50s due to the brush conformation of PEG, compared to the mushroom conformation of PEG on the surface of LNC100s (Figure 2.8) (147).

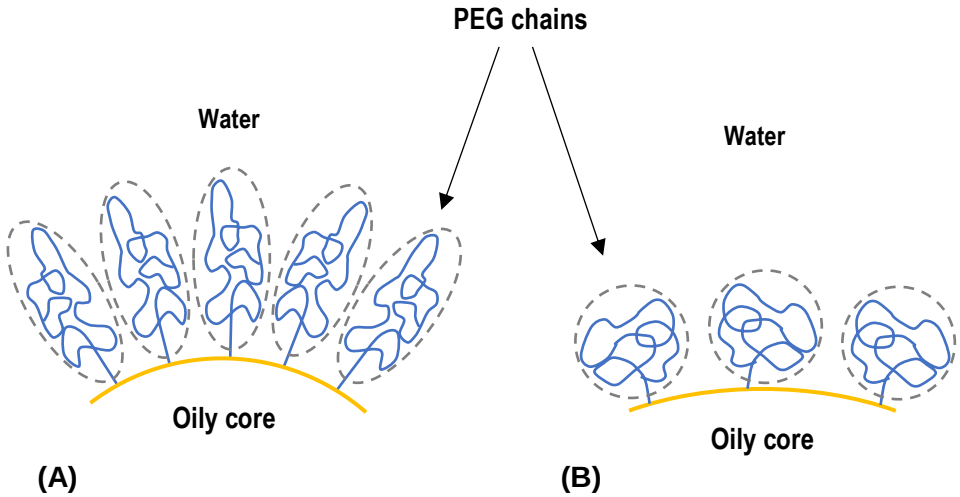

Figure 2.8. Schematic representation of PEG chains in (A) LNC50 with brush conformation and in (B) LNC100 with mushroom conformation

For liposome formulations, the presence of C6 ceramide markedly influenced the surface behaviour of lipid bilayer systems (Figure 2.9). At room temperature, no aggregation was observed for ghost liposome independently of salt concentration, though the size increased slightly, similar to LNCs formulations when exposed to the higher salt concentrations. In contrast, liposome-C6 experienced a sharp increase in size, ca. 5-fold

and 50-fold in 4 M and 5 M NaCl solutions, respectively. At 37°C, both ghost and C6 ceramide-loaded liposome exhibited massive aggregation when exposed to salt concentrations >2.5 M. The diameter of both liposome formulations increased ca. 20-fold in 4 M NaCl solutions 37°C. Meanwhile, in 5 M $NaCl_{aq}$ at 37°C, liposome-C6 experienced a slightly higher increase in diameter (ca. 60-fold) than ghost liposome (ca. 35-fold).

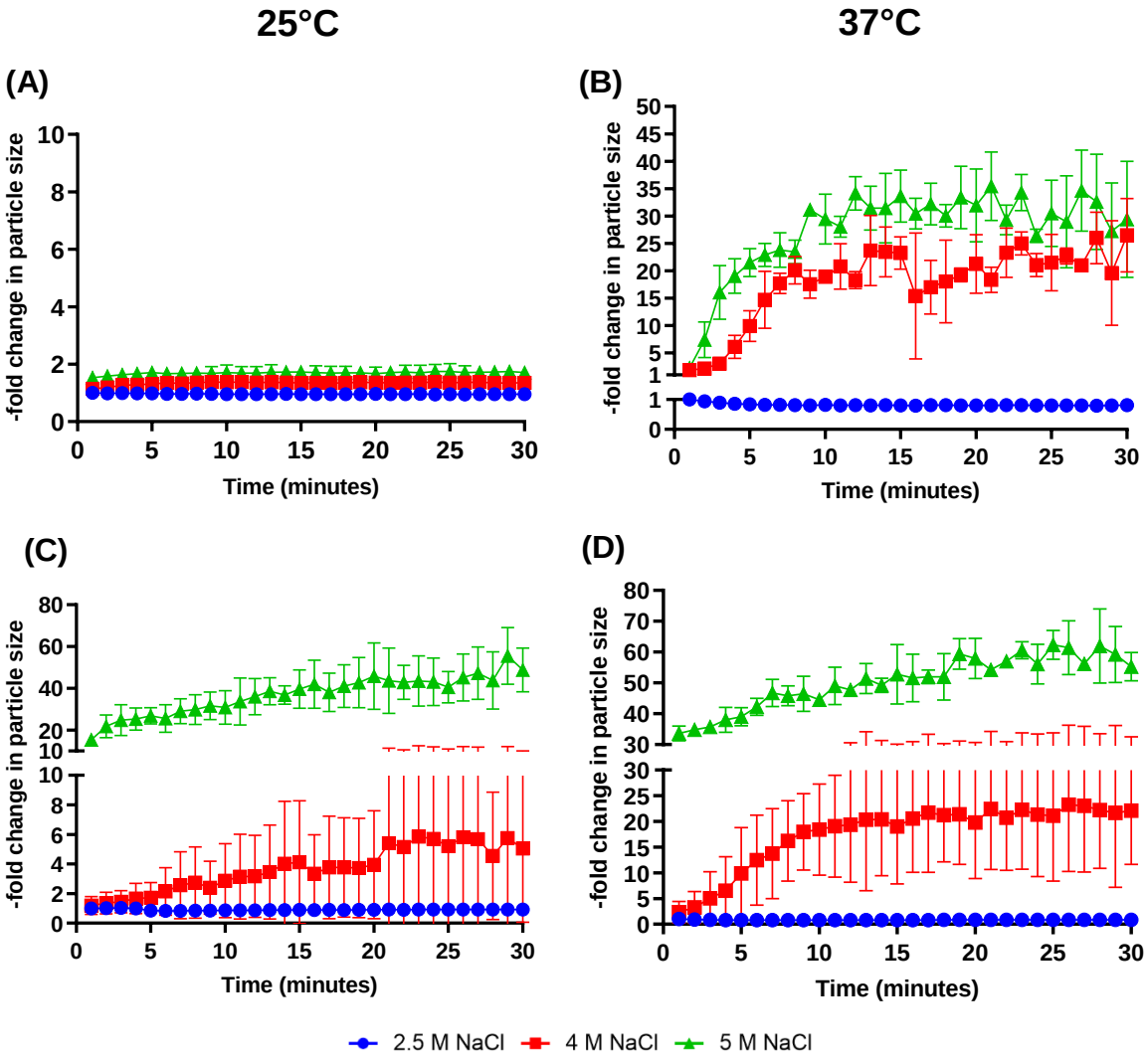

Figure 2.9. Salt aggregation test of liposomes at 25° and 37°C with (A,B) liposome-ghost; (C,D) liposome-C6. Data presented as mean ± SD from three individual batches (*n*=3). Statistical analysis using two-way ANOVA followed by a post-hoc Dunnett test, compared to the initial measurement at minute 0.

The SAT results confirm what was seen in the stability study, where C6 ceramide had an impact on the organisation of the lipid bilayer and potentially lowered the ability of PEG to protect the liposomes from aggregation. Yet, these results are also somewhat confounding, especially as the PEG chains used in liposome formulations are longer than for LNCs, which should be shielding the hydrophobic surface better (148,149). However, the conformation of PEG is likely to have had an impact, similar to what was discussed for LNCs. It is important to note that PEG was added to the lipid mixture during liposome formation, as opposed to inserted into pre-formed vesicles. The means that PEG chains will be found on both sides of the liposome bilayer, i.e. inner core and outer surface. Still, the density on the outer surface should be sufficient to shield the bilayer but may be too high to avoid PEG adopting a mushroom conformation. Further work may be needed to fully understand these results. Importantly, no significant change in size was observed at lower salt concentration ($\leq$ 2.5 M), which indicated all liposomes should be stable at physiological salt concentration (0.9% ~ 0.15 M).

2.4. Conclusion

LNCs and liposome with and without C6 ceramide were successfully prepared with a unimodal distribution. The presence of C6 ceramide did not have a major impact on the physico-chemical properties and surface hydrophobicity of LNCs but did affect the liposome formulation. Both sizes of ghost and ceramide-loaded LNCs had great colloidal stability under storage (4°C) and cell culture conditions. In contrast, stability under both conditions was suboptimal for liposomal ceramide. Interestingly, though ghost liposomes were relatively stable, they were more prone to aggregate than LNCs at high salt concentrations, even at room temperature. It could be suggested that the changes in conformation and

hydration of PEG chains on nanoparticle surface may influence the determination of hydrophobic nanoparticles. Therefore, the use of LNCs as an alternative to liposome for ceramide delivery has the potential to be developed and requires further investigation from cell-based study. However, it is important to note that ceramide loading and entrapment efficiency were not measured here (due to issues accessing the right facilities), thus those experiments will be needed to confirm these findings.

3. Cell Study

3.1. Introduction

Cellular interaction of nanoparticles has an important role in most drug delivery studies. Here, as nanoparticles act as carriers for the bioactive, pro-apoptotic sphingolipid, C6 ceramide, the cell studies were performed on cancer cells. In this study, MDA-MB-231 cells, a metastatic triple-negative breast cancer (TNBC) cell line, were used as a model. Currently, limited treatment options are available for TNBC since the cells do not express common receptors used for targeted, personalised medicines, such as the oestrogen (ER), progesterone (PR) and human epidermal growth factor receptors (HER2) (150–152). Furthermore, MDA-MB-231 is known to express multiple multidrug resistance (MDR) transporters, such as P-glycoprotein (P-gp) and breast cancer resistance protein (BCRP) (153,154). These efflux transporters naturally protect tumour cells by pumping out cytotoxic drugs leading to poor intracellular drug levels (155,156). Thus, inhibiting those transporters may help resolve some of the causes behind failure of chemotherapy in TNBC. Interestingly, exogenous C6 ceramide was reported to enhance the secretion of exosome-associated efflux transporters and reduce MDR which makes C6 ceramide beneficial as adjuvant drug therapy for TNBC (157). This mechanism may partially explain the ability of ceramide C6 to act in synergy with doxorubicin and paclitaxel, two known substrates of the P-gp, when used to treat MDA-MB-231 cells (49,50,52).

In vitro cytotoxicity of liposomes and LNCs was using Cell-Counting Kit 8 (WST-8/ CCK8). This colorimetric method is based on metabolic dyes, tetrazolium salt, which is reduced by cellular dehydrogenases to an orange formazan product that is soluble in cell culture medium (158). The amount of orange formazan is proportional to the number of viable and metabolic active cells. The CCK8 assay is a simpler assay compared to other

common tests, since it does not require an additional step to dissolve the formazan crystals, and as has a high sensitivity, stability and low toxicity compared to the other tetrazolium salt-based assays, such as MTT and XTT (158–161).

In order to probe the mechanism of cell death, the annexin V/ PI staining was performed in this study to determine whether C6 ceramide induced apoptosis. This assay is a firmly established *in vitro* cytotoxicity assay to differentiate between the early and late stages of apoptotic and necrotic cells following exposure to the nanoparticles. Apoptosis, also known as programmed cell death, is typically triggered by a normal physiological process in the body. There are several specific characteristics in apoptotic cells, including cell dehydration and shrinkage, nuclear fragmentation, lack of an inflammation response, and formation of apoptotic bodies (162–164). Apoptosis also occurs as a defence mechanism during healing process and beneficial to an organism (165). In comparison, necrosis, another mechanism of cell death is always pathological, and can be triggered by external factors, drugs or disease. Necrosis is characterised by cell inflammation, nuclear degradation, cell enlargement, leakage of content, and loss of membrane integrity (166,167). For cancer treatment, it is important to differentiate between both mechanisms. Most cancer therapies aim to induce apoptosis as elimination of cancer cells could be controlled without triggering inflammation response (163,165). Necrosis, on the other hand, provoke inflammation and leakage of cellular contents which could provide a condition for tumour metastatic (163,168).

In addition to the annexin V/ PI staining assay, the caspase-3/7 activity assay was also conducted in this study since the cells that undergo apoptosis are almost always correlated with the activation of the caspase signalling pathway (169,170). Caspase activation is an integral part of apoptotic cell death (165). First, the initiator caspases are activated, (caspase-

2, -8, -9, and -10) (171,172), then cleaved which then triggers the activation of effector caspases (caspase-3, -6, and -7) leading to cell apoptosis (Figure 3.1 A) (172–174). Although there are some similarities between caspase-3 and 7, both have distinct functions in apoptosis. Morphologic changes and DNA fragmentation in apoptotic cells are mainly controlled by caspase-3, while caspase-7 is responsible for reactive oxygen species (ROS) production and helps in cell detachment (175,176).

Flow cytometry was used to study both mechanism of cell death and caspase activity. In brief, the interactions between nanoparticles and cells in term of toxicity and cellular death mechanism are presented from these results of the cell-based study.

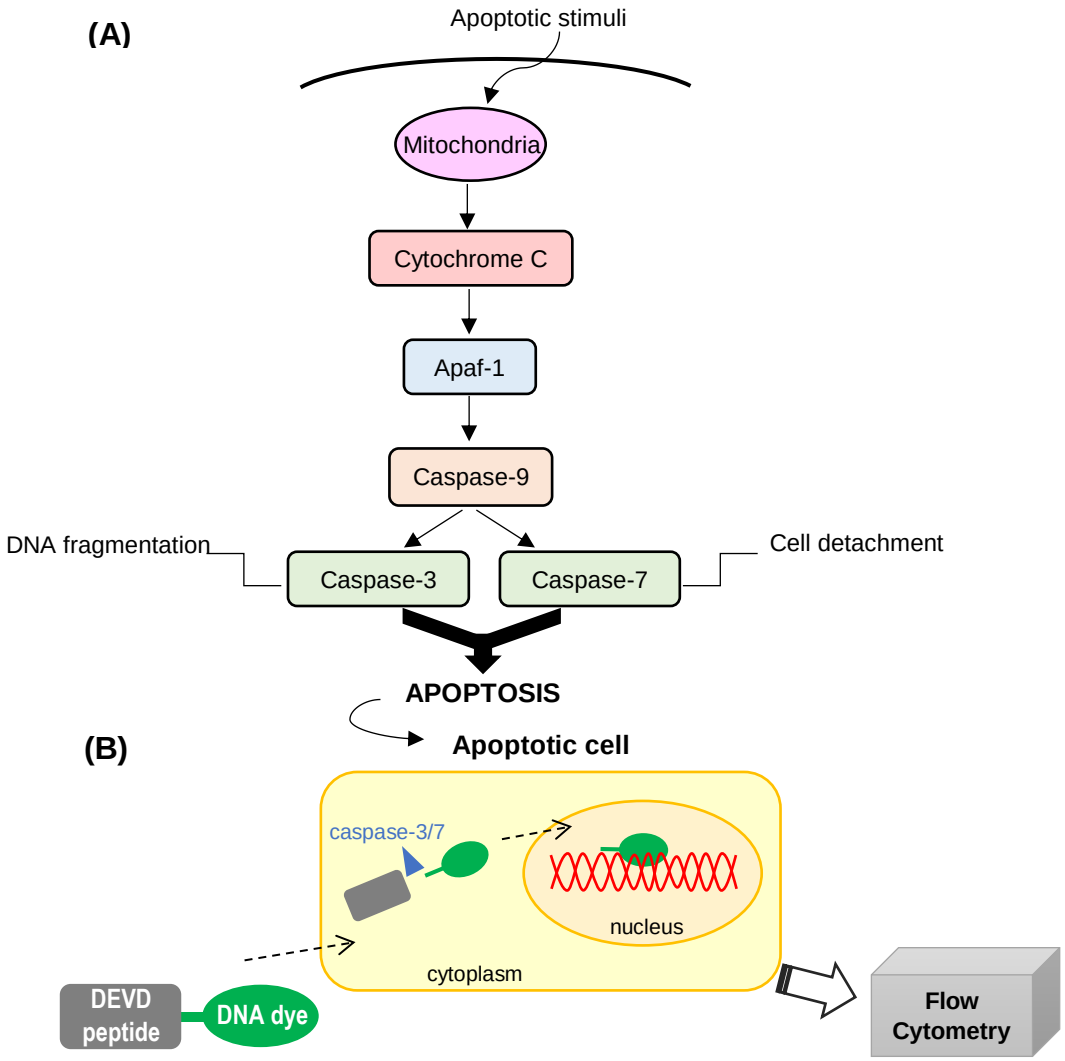

Figure 3.1. Schematic figure of apoptosis cell death pathway with (A) caspase cascade activation and (B) caspase-3/7 assay principle; adapted from (176,177) with permission from Springer Nature and Cold Spring Harbor Laboratory Press. Caspase-3/7 recognizes and cleaves the DEVD peptide which is a caspase-3/7 specific sequence that is couple with a DNA probe. When the probe enters the cell nucleus, it binds to the DNA thus producing a fluorescence signal and captured by flow cytometry.

3.1.1. Aim and objectives

This chapter will focus on the cellular characteristics of two specific nanocarriers (LNCs and liposome) for C6 ceramide delivery towards MDA-MB-231 cells. The main aim is to determine whether encapsulation will affect the pharmacological activity of C6 ceramide, and to examine the following additional hypotheses:

1. C6 ceramide-containing nanoparticles (LNCs-C6 and liposome-C6) will be more cytotoxic than the equivalent ghost-nanoparticles (LNCs-ghost and liposome-ghost).
2. C6 ceramide-containing nanoparticles (LNCs-C6 and liposome-C6) will induce apoptotic cell death to a greater extent than the equivalent ghost-nanoparticles (LNCs-ghost and liposome-ghost).

Objectives

1. Cytotoxicity assessment of the nanoparticles with and without ceramide against MDA-MB-231 cells using CCK-8 assay.
2. Analysis of cell death mechanism induced by C6 ceramide in MDA-MB-231 cells using annexin V/ PI staining assay by flow cytometry.
3. Analysis of caspase-3/7 activity to probe the mechanism action of C6 ceramide in inducing apoptosis using CellEvent™ caspase-3/7 green flow cytometry assay kit.

3.2. Materials and methods

3.2.1. Materials

Dulbecco's Modified Eagle Medium (DMEM) - high glucose, Dulbecco's phosphate buffered saline (DPBS), penicillin-streptomycin (10,000 U/mL), heat-inactivated foetal bovine serum (HI FBS) and TrypLE™ express enzyme were purchased from Thermo Fisher Scientific Ltd. (Loughborough, Leicestershire, UK). Cell Meter™ Colorimetric WST-8 Cell Quantification Kit (CCK-8) was purchased from AAT Bioquest, Inc. (Pleasanton, California, US). Staurosporine was purchased from Cambridge Bioscience Ltd. (Cambridge, UK). Dead Cell Apoptosis Kit using Annexin V Alexa Flour 488 & Propidium Iodide, as well as CellEvent™ Caspase-3/7 Green Flow Cytometry Assay Kit were purchased from Thermo Fisher Scientific (Invitrogen, UK).

3.2.2. Methods

3.2.2.1. Cell culture

MDA-MB-231 triple negative breast cancer cells were grown in DMEM high glucose supplemented with 10% foetal bovine serum (FBS) and 1% penicillin-streptomycin (500 U/mL). Cells were maintained at 37ºC in humidified air with 5% CO_2. The cells were sub-cultured when its confluency reached ~80% using TrypLE™ express enzyme. The passage number of the cells used for this study was 39 to 48.

3.2.2.2. Cytotoxicity assay

The cytotoxicity of the nanoparticles (with and without ceramide) and free-C6 ceramide was evaluated by using the CCK-8 assay. The cells were seeded into 96-well plate (flat-bottom) at density 1 x 10^4 cells per well in 200 µL cell culture medium for 24 hours before treatment. The cells (same passage) were then treated with three individual nanoparticle batches with several different concentrations for 24, 48 and 72 hours (37ºC, 5% CO_2, 100% humidity). The nanoparticles concentrations used were 0.04 – 5 mg/mL and 0.005 – 5 mg/mL, which are equivalent to ceramide concentrations (0.4 – 50 µM and 0.95 – 945 µM) for LNCs and liposomes, respectively. At the end of incubation, the medium was aspirated, and the cells were washed using DPBS and replenished with 100 µL medium containing 10 µL of CCK-8 solution per well. The plates were incubated at 37ºC for 2 hours and measured the absorbance using microplate reader (Fluostar Omega, BMG Labtech, Aylesbury, UK) at wavelength 460 nm. The percentage of cell viability was calculated using this following equation:

$$\%\ \text{Cell Viability} = \frac{\text{OD treatment} - \text{OD positive control}}{\text{OD untreated} - \text{OD positive control}}\ \text{x}\ 100\%$$

*OD: optical density obtained from absorbance value recorded in the instrument

3.2.2.3. Apoptosis assay

The Annexin V / PI staining assay was performed according to the instructions of the manufacturer. Briefly, MDA-MB-231 cells were seeded at 1.0 x 10^5 cells/ well in 12-well plate and grown for 48 hours in complete cell culture media. Cells were then treated with ghost nanoparticles or C6-containing nanoparticles for 24 hours in complete cell culture media. Following treatment, floating cells were collected, and adherent cells were harvested by trypsinization. After the cells were washed twice with cold PBS, the pelleted cells were resuspended in 1X-annexin binding buffer to reach the cell density ca.1 x 10^6 cells/mL, and then stained using Alexa Fluor 488 Annexin V and PI (Propidium Iodide) and incubated for 15 minutes at room temperature. After the incubation period, the stained cells were immediately analysed by flow cytometry. The fluorescence emission was measured at 530 nm and 575 nm (or equivalent) using 488 nm excitation. Viable cells were double negative, early apoptotic cells were annexin V positive and negative for PI staining, and late apoptotic cells were double positive.

3.2.2.4. Caspase-3/7 assay

Caspase-3/7 enzymatic activity in apoptotic cells was detected using the CellEvent™ caspase-3/7 green flow cytometry assay kit and performed according to the instruction of the manufacturer. Briefly, MDA-MB-231 cells were seeded at 1.0 x 10^5 cells/ well in 12-well plate and grown for 48 hours in complete cell culture media. Cells were then treated with ghost nanoparticles or C6-containing nanoparticles for 24 hours in complete cell culture media. Cells were harvested after incubation period and adjusted the cell concentration between 1 x 10^5 cells/ml and 1 x 10^7 cells/mL using DPBS. CellEvent caspase-3/7 green detection reagent was then added into the flow cytometry

tubes each containing 1 ml of cell suspension and incubated for 60 minutes at room temperature, protected from the light. During the last 5 minutes of staining, SYTOX AADvanced dead cell stain in DMSO was added to the sample tubes and mix gently. The samples were analysed without washing or fixing, using 488 nm excitation and collecting fluorescence emission using a 530/30 bandpass filter or equivalent for CellEvent caspase-3/7 green detection reagent and a 690/50 bandpass filter or equivalent for SYTOX AADvanced dead cell stain. The detection of activated caspase-3 and -7 in apoptotic cells with CellEvent caspase-3/7 green fluorescence positive and negative for SYTOX AADvanced can easily be discriminated from live and necrotic cells.

3.2.2.5. Data processing and statistical analysis

Data processing, graph, and statistical analysis were performed using GraphPad Prism version 9 (GraphPad Software Inc., California, USA). Cytotoxicity, apoptosis, and caspase data were analysed using two-way ANOVA. Flow cytometry data were processed using CytExpert version 2.5 (Beckman Coulter Inc., California, USA).

3.3. Results and discussion

3.3.1. Cytotoxicity of LNCs and liposomes (with and without C6 ceramide)

The viability of MDA-MB-231 breast cancer cells following exposure to ghost-nanoparticles (LNCs-ghost and liposome-ghost) and C6-loaded nanoparticles (LNCs-C6 and liposome-C6) at various time points are displayed in Figure 3.2. All formulations presented concentration- and time-dependent toxicity with the longer exposure times and higher nanoparticle concentrations leading to noticeable decreases in cell viability. As expected, ghost nanoparticles were less toxic than C6-loaded nanoparticles at the same

particle concentrations. Here, adding C6 ceramide to nanoparticle formulations did not have a major impact on the cytotoxicity of LNCs, but did affect the toxicity of liposomes. Indeed, though statistically significant, the change in IC50 between ghost and C6-loaded nanoparticles was more noticeable for liposomes compared to LNCs; this might be due to the low inherent toxicity of ghost liposomes towards MDA-MB-231 cells (Table 3.1). In contrast, ghost LNCs may be naturally more toxic due to the presence of surfactant (80,81,178,179). Although the purification process has been performed, surfactant molecules may still be released from the LNC surface to cause some toxicity (78). This phenomenon has also been reported in literature (78,80,81).

Furthermore, these results were in line with previous reports that ghost liposomes had no effect on the cytotoxicity of MDA-MB-231 (31), compared to ghost LNCs (126). The higher toxicity of LNCs must be considered against the fact that HS-PEG was reported to inhibit the P-gp which could help overcome drug resistance in several cancer cells, including TNBC cells (78,79).

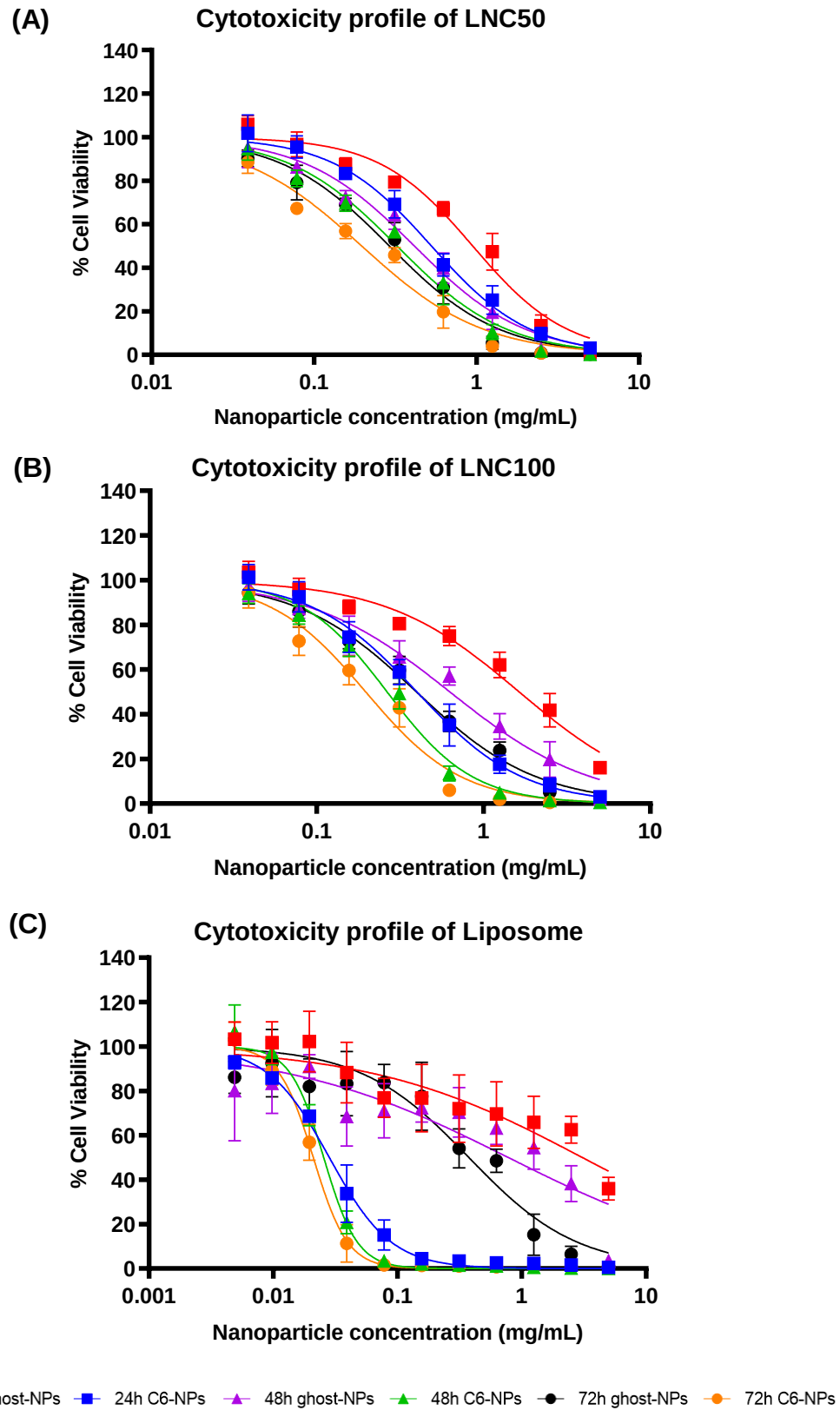

Figure 3.2. Cell viability of MDA-MB-231 following exposure to nanoparticles (NPs) with and without C6 ceramide with (A) LNC50; (B) LNC100; (C) liposome. Data are presented as mean ± SD from three individual nanoparticle batches (*n*=3).

Table 3.1. IC50 of nanoparticles with and without C6 ceramide on MDA-MB-231 cells

Exposure time (hours)	IC50 (mg/mL)					
	LNC50-ghost	**LNC50-C6*****	**LNC100-ghost**	**LNC100-C6*****	**Liposome-ghost**	**Liposome-C6*****
24	0.95 ± 0.14	0.53 ± 0.06	1.64 ± 0.30	0.40 ± 0.05	3.09 ± 1.87	0.029 ± 0.003
48	0.42 ± 0.07	0.32 ± 0.05	0.63 ± 0.12	0.26 ± 0.02	0.79 ± 0.59	0.025 ± 0.002
72	0.29 ± 0.05	0.20 ± 0.03	0.40 ± 0.05	0.20 ± 0.03	0.38 ± 0.10	0.021 ± 0.001

(1)Data are presented as mean ± SD from three individual nanoparticle batches (n=3)
(2)Statistical analysis using two-way ANOVA compared ghost nanoparticles to C6-loaded nanoparticles. Significant differences were observed in all formulations ($^{***}p<0.001$)

In order to evaluate the ability of cells to recover after exposure to the ghost nanoparticles, a cell recovery assay was conducted. After 24 hours of treatment with the ghost nanoparticle, the culture media was changed and cells were left to recover for 48 and 72 hours (Figure 3.3). The results suggested that for cells exposed to LNC50s, growth rates were initially slower (ca. 1.5-fold) than the expected doubling time of MDA-MB-231 cells (ca. 36 hours), even at concentrations below the IC50 (0.95 ± 0.14 mg/mL). However, the growth rates were back as expected (ca. 4-fold) within 72h, except for the highest concentration where no growth was seen. For LNC100s, the growth rates were higher than expected with ca. 3- to 5.5-fold increases in number within 48 – 72h. Meanwhile, cells treated with liposomes grew at the expected rate, ca. 2-fold increase in number after 48h and ca. 4.5-fold increase within 72h.

The ability of MDA-MB-231 cells to recover was increased in the order following exposure to LNC50-ghost < liposome-ghost < LNC100-ghost. Somewhat expectedly, cells treated with LNC50 possess the lowest recovery and, at the highest particle concentration (2.5 mg/mL) cells failed to recover. On the other hand, cells treated with LNC100s made the most significant recovery, even at concentrations higher than their IC50 (1.64 ± 0.30

mg/mL). Interestingly, cells recovered better from exposure to ghost LNC100s than exposure to ghost-liposomes. This was somewhat unexpected but may be due to the smaller-sized liposomes (ca. 70 vs 100nm) being able to penetrate deeply and bind more strongly to the cells (180–182). The results may need to be investigated further since the specific cell responses after exposure to nanoparticles are complex and determined by numerous factors. Indeed, the behaviour of drug delivery systems not only depends on nanocarrier intrinsic properties, but also involves different mechanisms and signalling pathways (183–185).

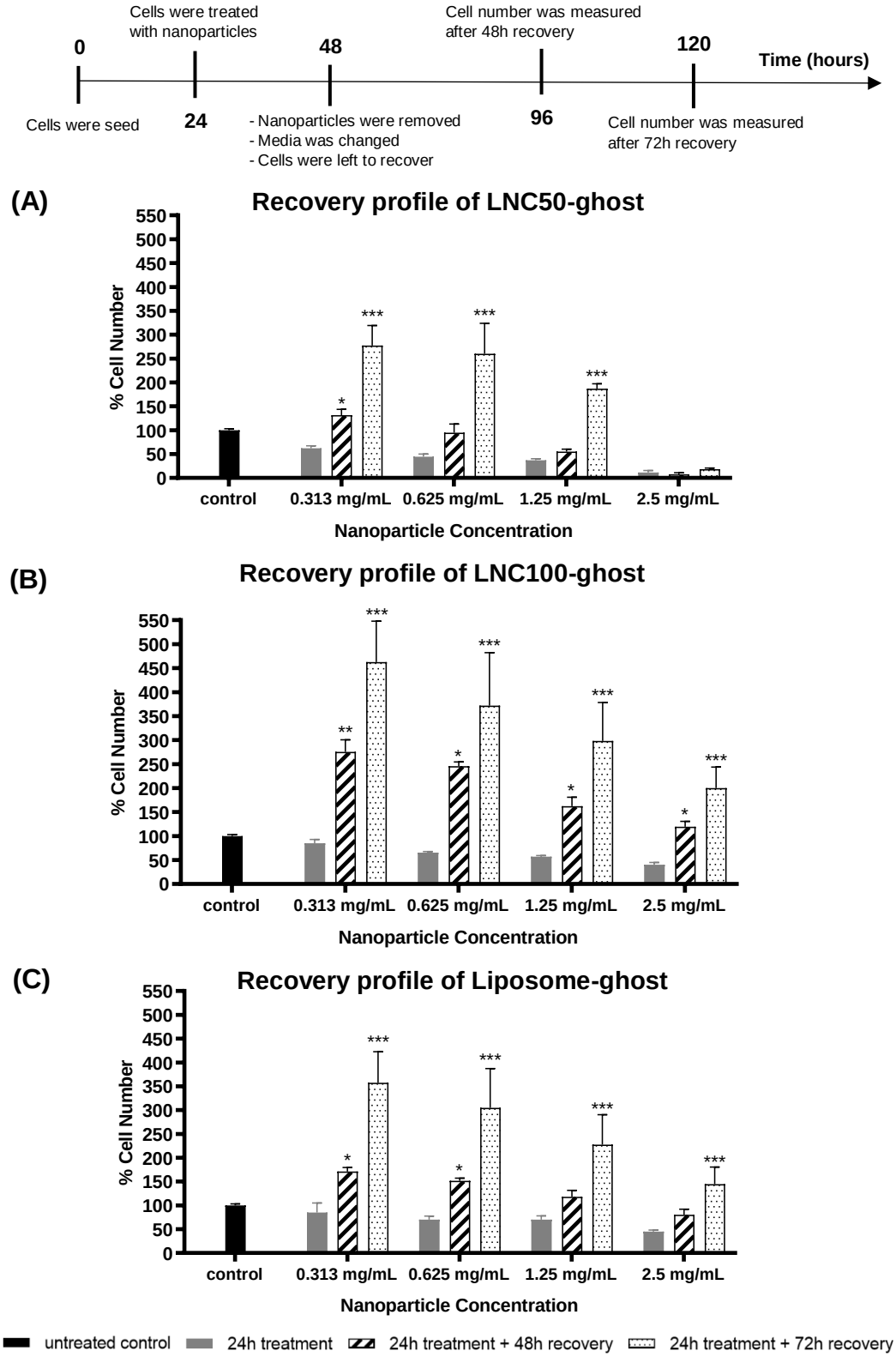

Figure 3.3. The ability of MDA-MB-231 cells to recover from 24h exposure to nanoparticles (A) LNC50-ghost; (B) LNC100-ghost; (C) liposome-ghost. Data are presented as mean ± SD from three individual nanoparticle batches (n=3). Statistical analysis using one-way ANOVA followed by a post-hoc Dunnett test compared to 24h treated cells at the same given concentration ($^{*}p<0.05$, $^{**}p<0.01$, $^{***}p<0.001$).

C6 ceramides have been reported to diffuse spontaneously across the cellular membrane (31,33). Therefore, to assess the impact of encapsulation, the cytotoxicity assay was also performed with free-C6 ceramide on TNBC cells. The results revealed that free-C6 and C6-loaded nanoparticles exhibited identical dose-response profiles after 24h of treatment. Increasing exposure time to 48 or 72h revealed some differences, with LNC-encapsulated C6 showing slightly higher toxicity, especially at low C6 concentrations, and liposomal C6 having the lowest toxicity (Figure 3.4). It is important to note that the cytotoxicity of LNCs-C6 was limited by the toxicity of the particles themselves and it was not possible to test C6 concentrations beyond 50 μM.

Here, no noticeable difference was observed in the IC50 between free-C6 and C6-loaded nanoparticles, except for liposome-C6 (Table 3.2). Though the IC50 of liposome-C6 was statistically significant, the values were within the same order of magnitude and the differences seen may not be clinically-relevant. These results indicated that encapsulation maintained the efficacy of C6 ceramide on MDA-MB-231 cells. For LNCs, the possibility of an additive effect between LNCs and C6 ceramide may need to be explored further.

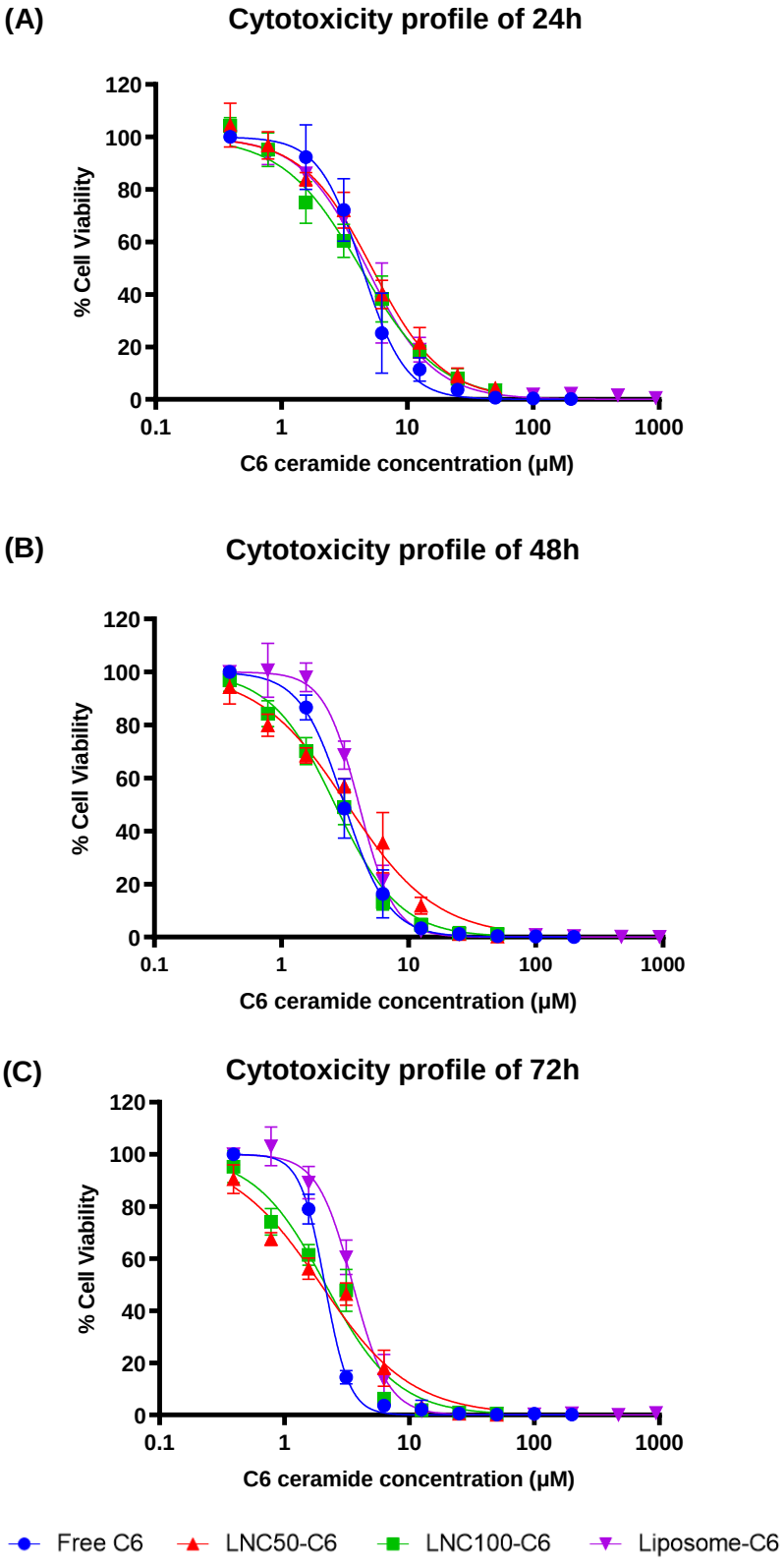

Figure 3.4. Cell viability of MDA-MB-231 following exposure to free-C6 ceramide and C6-loaded nanoparticles at different time points (A) 24h; (B) 48h; (C) 72h. Data are presented as mean ± SD from three biological replicates (*n*=3).

Table 3.2. IC50 of free-C6 and C6-loaded nanoparticles on MDA-MB-231 cells

Exposure time (hours)	IC50 (µM)			
	Free-C6	**Liposome-C6*****	**LNC50-C6**	**LNC100-C6**
24	4.41 ± 0.75	5.53 ± 0.52	5.27 ± 0.60	4.01 ± 0.48
48	3.13 ± 0.34	4.80 ± 0.31	3.24 ± 0.46	2.64 ± 0.23
72	2.11 ± 0.11	3.79 ± 0.21	1.96 ± 0.32	1.97 ± 0.29

(1)Data are presented as mean ± SD from three individual nanoparticle batches (n=3)
(2)Statistical analysis using two-way ANOVA compared free-C6 to C6-loaded nanoparticles. Significant difference was observed in liposome-C6 ($^{***}p<0.001$)

For liposome-C6, uptake is projected to occur *via* spontaneous exchange of the ceramides between particles and the cellular membrane (Figure 3.5) as reported previously (31,33,133,186). Meanwhile, for LNCs, ceramide uptake is predicted to happen either through endocytosis and intracellular release of encapsulated ceramides, or *via* spontaneous exchange of C6 ceramide chains released into the extracellular environment. However, it remains unclear whether the PEG chains found on both liposome and LNC surface could interfere with these transfer mechanisms. Therefore, the uptake mechanism of C6-loaded nanoparticles may need to be investigated further.

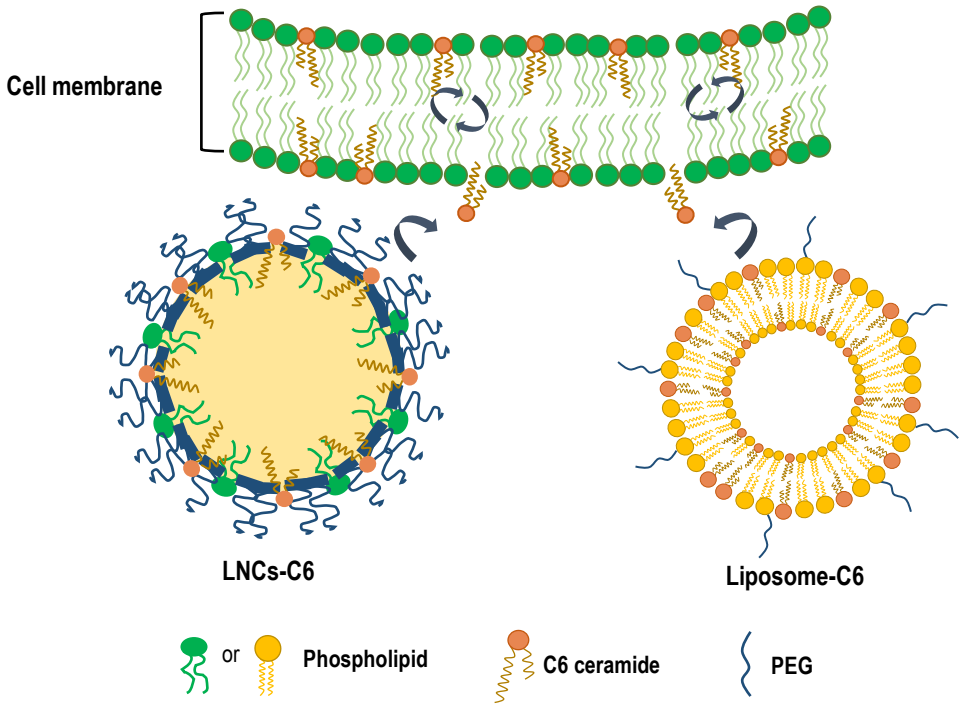

Figure 3.5. Schematic representation of ceramide bilayer exchange mechanism from LNCs-C6 and liposome-C6 into cell membrane, adapted from (133) with modification and permission of Am Soc for Pharmacology & Experimental Therapeutics.

3.3.2. Apoptosis assay

A flow cytometry annexin V/ PI staining assay was performed to confirm the pro-apoptotic activity of C6 ceramide was maintained after encapsulation. In live cells, phosphatidylserine (PS) is present in the inner leaflet of the plasma membrane (166,187,188). In the early stage of apoptosis, PS is translocated from the inner to the outer leaflet of the plasma membrane, where it can bind to annexin V, resulting in an increased in the signal in flow cytometry (189–191). As cells proceed to later stages of apoptosis or in case of necrosis, the integrity of the plasma membrane becomes affected, allowing the uptake of propidium iodide (PI), thus producing red fluorescence signal (190–192); viable cells with intact membranes will exclude both PI and annexin V. Therefore, the viable cells are both annexin V and PI negative (lower left quadrant/ Q4), early apoptotic cells are

annexin V positive and PI negative (lower right quadrant/ Q3), and late apoptotic cells are double positive (upper right quadrant/ Q2) (31,167,190). Meanwhile, necrotic cells are PI positive and annexin V negative (upper left quadrant/ Q1).

Here, two concentrations of C6 ceramide were tested for apoptosis, 12.5 μM and 25 μM. Preliminary data showed that lower concentration (3.13 μM) did not induce apoptosis, whilst higher concentrations (>25 μM) caused massive cell death (data not shown). In addition, a concentration of 25 μM has been reported to be sufficient to induce apoptotic cell death on MDA-MB-231 (31).

Untreated cells and cells treated with staurosporine (STS) were also used in this study as negative and positive control, respectively (Figure 3.6). There were shifts in cell population from the live cells to the early and late apoptotic cells for C6 ceramide-containing nanoparticles compared to the ghost nanoparticles at the same nanoparticle concentrations (Figure 3.7 – 3.9). It is important to notice that the percentage of cell viability was different between CCK-8 and apoptosis assay at the same concentrations due to differences in experimental design and cell density used. However, although the percentages of live cells were slightly different, the trend remained the same where LNC50s had the highest toxicity, followed by LNC100 and liposome.

The proportion of apoptotic cells increased remarkably from 2.92% (untreated) to 44.80% (STS) which confirmed that this assay worked properly (Figure 3.6). No significant change in the number of apoptotic cells was seen for ghost nanoparticles compared to the negative control, except for LNC50-ghost (Figure 3.7–3.9). Higher surfactant content in LNC50 was reported to potentially promote apoptotic cell death (193). This result clearly indicated that ghost nanoparticles act as a baseline in this experiment. Furthermore, differences were observed between ghost nanoparticles and C6-loaded nanoparticles for all

formulations in a concentration-dependent manner. For instance, the proportion of apoptotic cells increased from 8.43% and 15.93% (LNC100-ghost) to 16.30% and 41.38% (LNC100-C6) at equivalent concentrations (Figure 3.8). Moreover, though the size was similar, ghost liposomes did not induce apoptosis to the same extent as LNC50s (2-3% vs. 16-58%), again, likely due to the high surfactant content.

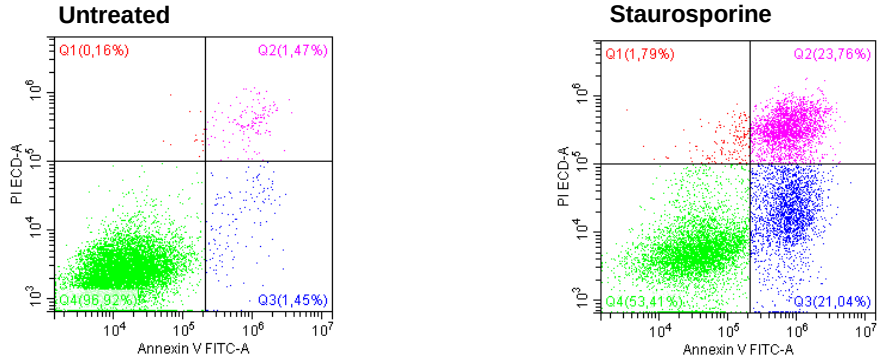

Figure 3.6. Representative flow cytometry dot-plots of untreated MDA-MB-231 cells and after 24h of treatment with staurosporine stained with annexin V/ PI.

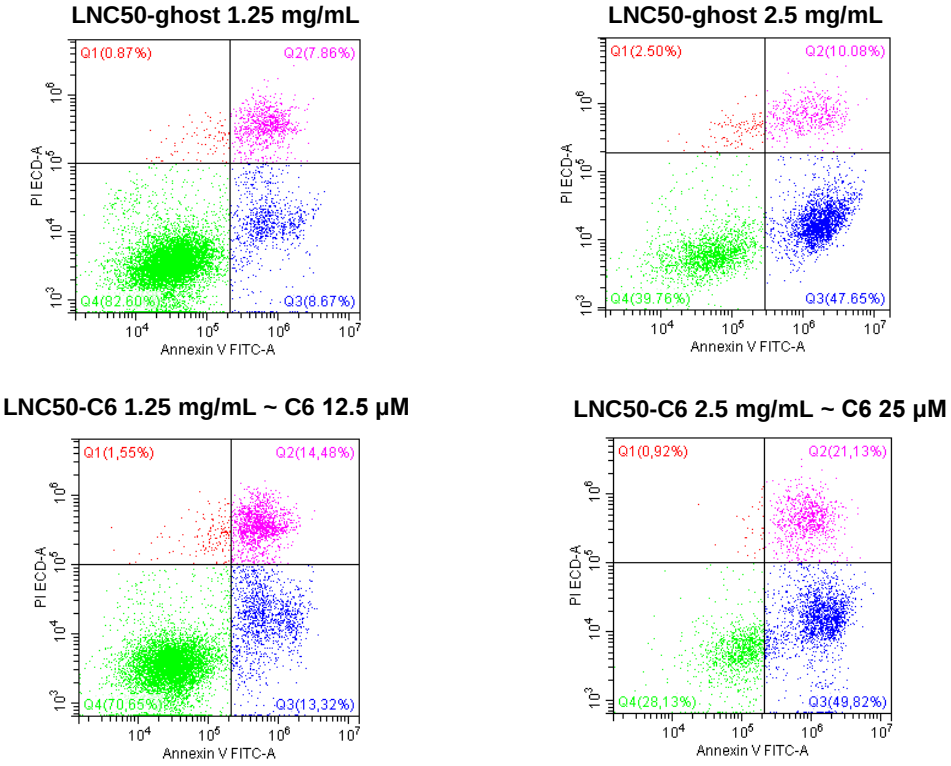

Figure 3.7. Representative flow cytometry dot-plots of MDA-MB-231 cells stained with annexin V/ PI after 24h of treatment with LNC50 with and without C6 ceramide at the same nanoparticle concentrations (mg/mL) or equivalent to ceramide content (µM) in LNC50-C6.

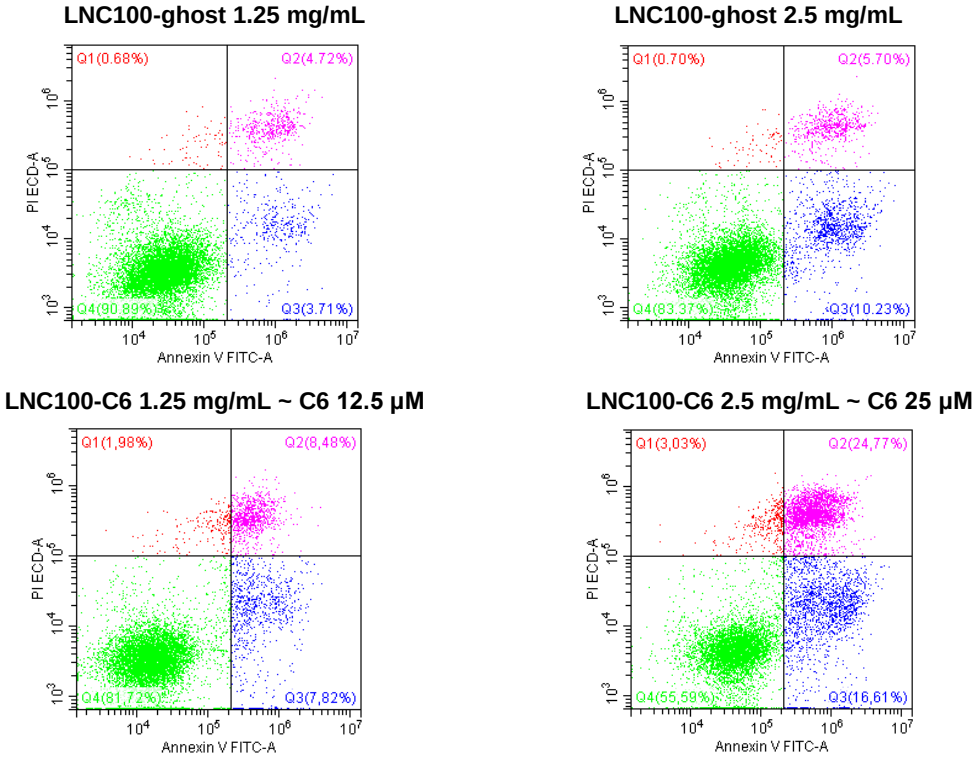

Figure 3.8. Representative flow cytometry dot-plots of MDA-MB-231 cells stained with annexin V/ PI after 24h of treatment with LNC100 with and without C6 ceramide at the same nanoparticle concentrations (mg/mL) or equivalent to ceramide content (µM) in LNC100-C6.

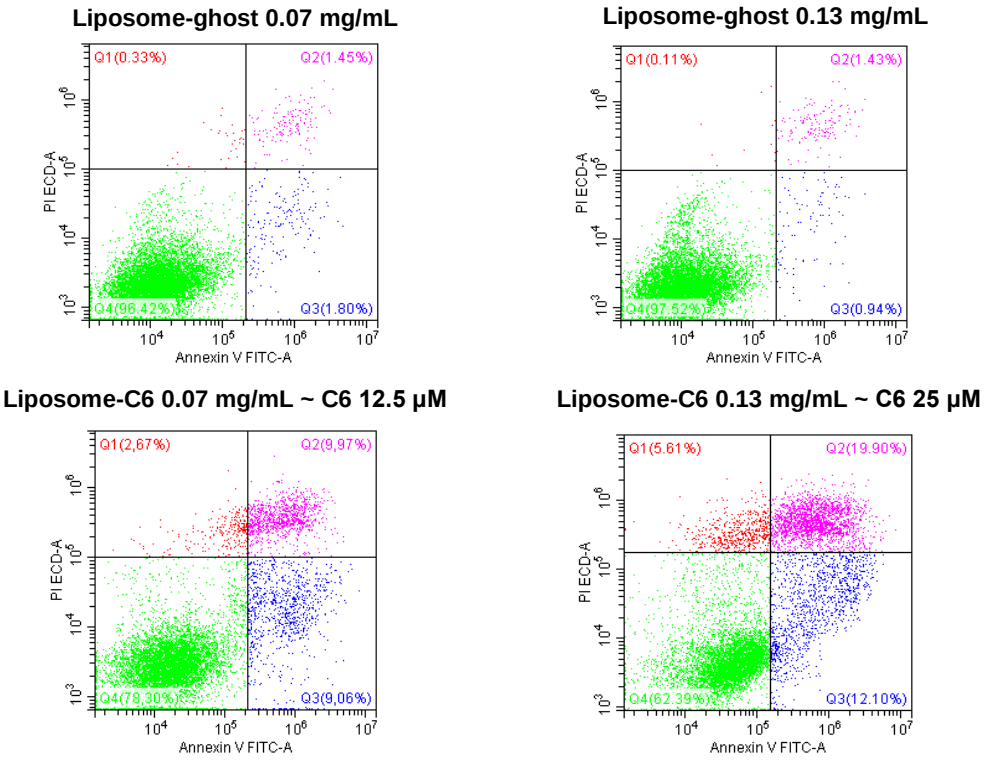

Figure 3.9. Representative flow cytometry dot-plots of MDA-MB-231 cells stained with annexin V/ PI after 24h of treatment with liposome with and without C6 ceramide at the same nanoparticle concentrations (mg/mL) or equivalent to ceramide content (µM) in liposome-C6.

To evaluate the impact of encapsulation, the same assay was performed with free C6 ceramide (Figure 3.10). The results revealed that both the dose and formulation of ceramide had an impact on pro-apoptotic activity (Figure 3.11). Moreover, at the higher dose, LNC-encapsulated C6, especially LNC50-C6, inducing a stronger pro-apoptotic, whereas liposome-C6 was less effective than free-C6. This result was in line with the cytotoxicity assay and suggested that liposome did not offer a considerable therapeutic benefit to the already active short-chain ceramide, compared to the LNCs. Previously, it was confirmed that C6-loaded liposome with the same ceramide loading (15 mol%) neither improved toxicity nor pro-apoptotic effect of ceramide towards breast cancer cells (MDA435/LCC6) (33). Although promising, more work will be needed to confirm these findings in *in vivo* models.

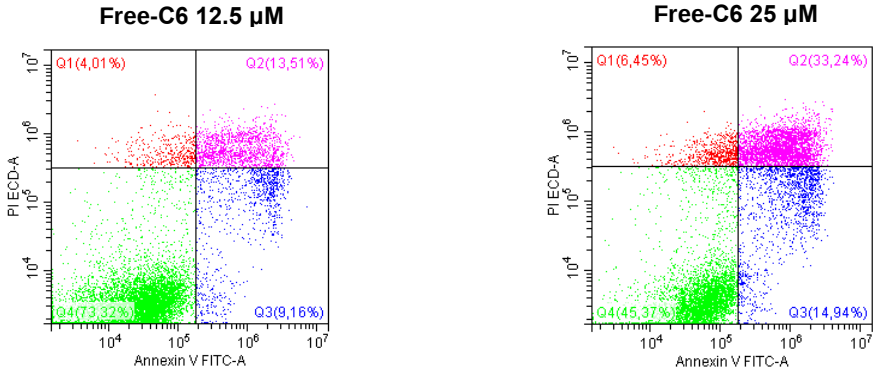

Figure 3.10. Representative flow cytometry dot-plots of MDA-MB-231 cells stained with annexin V/ PI after 24h of treatment with free-C6 ceramide.

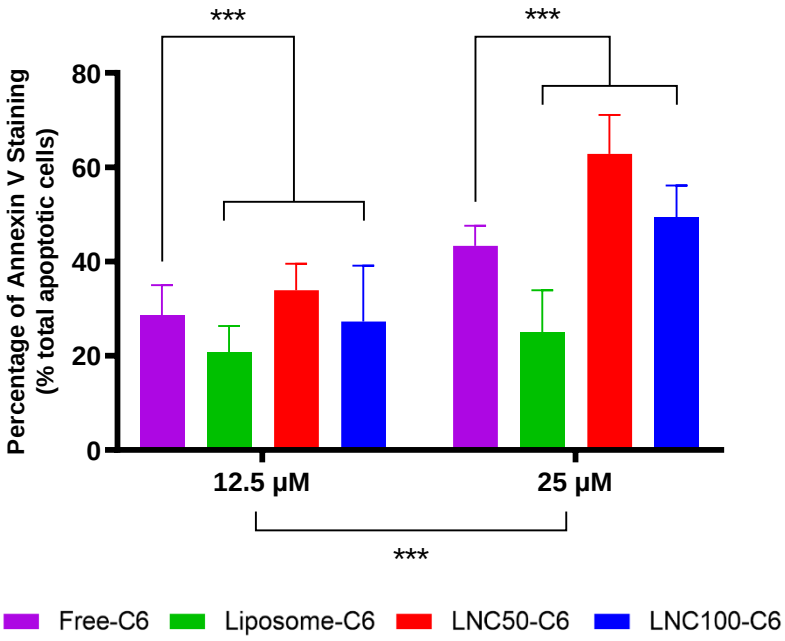

Figure 3.11. The percentage of annexin V positive cells after 24h of treatment with free-C6 and C6-loaded nanoparticles. Data are presented as mean ± SD from three individual batches (n=3). Statistical analysis using two-way ANOVA ($^{***}p<0.001$ for formulation and dose; $p>0.005$ for interaction).

3.3.3. Caspase-3/7 activity assay

Caspase assay was performed to further confirm the annexin V data. The main issues with annexin V assay are related to specificity and selectivity (165,194). Annexin V/ PI staining cannot completely discriminate between late-stage apoptosis and necrosis cells (195,196). Meanwhile, activation of caspase-3/7 occurs in the late apoptotic cells and is a more specific marker of the apoptosis response (197). In addition, there are no washing steps in the caspase kit protocol, but this is required in annexin V/ PI protocol which can lead to cell lost and damage. Thus, the annexin V data may not reflect the actual event of apoptosis (198).

Method optimisation has been done to identify the most suitable concentrations for this experiment. Lower concentrations were used (5 μM and 15 μM) to ensure sufficient cell numbers for analysis.

Caspase-3/7 activity increased in a concentration-dependent manner for all formulations. The differences in caspase activation were observed between ghost nanoparticles and C6-loaded nanoparticles at both concentrations (Figure S2 an S3 in supplementary information). Similar to annexin V assay, ghost nanoparticles were used as a control in this study to make sure that nanoparticles themselves had no big impact on caspase activation; this was true for LNC100-ghost and liposome-ghost but not for LNC50-ghost.

It has been widely reported that free C6 ceramide can induce mitochondrial dysfunction (32,199,200). Therefore, the same assay was carried out with free and encapsulated C6 ceramide to investigate the impact of formulation. The results showed that both dose and formulation of ceramide affected its efficacy in caspase activation (Figure 3.12). Interestingly, the difference between free-C6 and C6-loaded nanoparticles was less striking than for the annexin V data. LNC50 induced caspases to a higher extent comparable to free-C6, whilst LNC100-C6 and liposome-C6 both produced a similar response to free C6 ceramide.

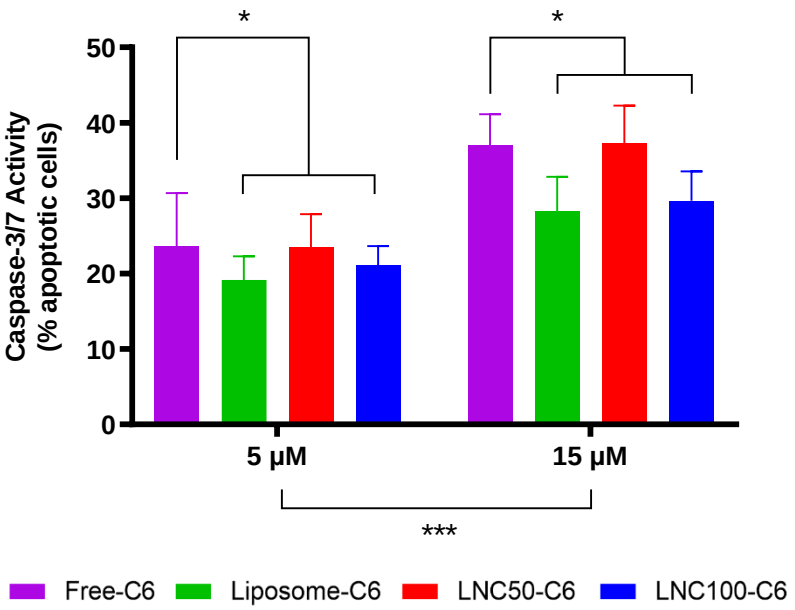

Figure 3.12. The percentage of caspase-3/7 activity positive response after 24h of treatment with free-C6 and C6-loaded nanoparticles. Data are presented as mean ± SD from three individual batches (n=3). Statistical analysis using two-way ANOVA ($^{*}p<0.05$ for formulation, $^{***}p<0.001$ for dose, $p>0.005$ for interaction).

To some extent, the results obtained here contradict previous reports that liposomal C6 could activate caspases to a greater extent compared to free-C6 at a concentration of 15 µM (31). As actual ceramide loading was not tested here, additional experiments will be needed to explain why different results were obtained. This indicates one of the limitations of the current study where dose calculations are based on the assumption of 100% entrapment efficiency and highlight the importance of ceramide quantification to confirm these preliminary findings.

3.4. Conclusion

The assessment of LNCs and liposome with and without ceramide revealed a time- and concentration-dependent cytotoxicity. Introducing C6 ceramide had a weaker impact on the toxicity of LNCs compared to liposome but C6-loaded nanoparticles were generally more toxic than the equivalent ghost nanoparticles. Mechanistic studies suggested that apoptosis through caspase activation was the main cell death mechanism. Formulating C6-ceramide as nanoparticles did not negatively affect its pharmacological activity towards MDA-MB-231 cells. Here, LNCs-C6 were slightly more effective than liposome-C6, however, further assessment is required to complement this study, including ceramide quantification and uptake studies. The former assay may also be useful for adjusting the dose of nanoparticles in future *in vitro* and *in vivo* studies.

4. Conclusion and Future Work

4.1. Conclusion

Even though C6 ceramide is an active pro-apoptotic sphingolipid, its unfavourable properties, such as poor-water solubility and susceptibility to enzymatic degradation, limit its therapeutic application. Therefore, ceramide encapsulation in nanoparticles will be required to increase intracellular levels and generally enhance its efficacy. In this study, encapsulation in LNCs provided a suitable alternative to liposomes for ceramide delivery, compared to liposomes which have been extensively proposed for that purpose previously.

4.1.1. The presence of C6 ceramide had no major effect on the physico-chemical properties of LNCs but had a noticeable impact on liposomes.

The physico-chemical properties of LNCs and liposomes were compared before and after addition of C6 ceramide. For the LNCs, two different sizes (50 nm and 100 nm) were prepared using a phase-inversion temperature method. Purification was a critical step in LNCs manufacture to remove the excess surfactant which could affect their cytotoxicity. Both sizes of LNCs with and without ceramide had excellent colloidal stability at 4°C and under cell culture conditions. In contrast, ceramide decreased the stability of liposomes under all conditions tested. Moreover, liposomes were more susceptible to precipitate than LNCs at high salt concentrations.

4.1.2. Cytotoxicity and pro-apoptotic activity of C6 ceramide is maintained after encapsulation in LNCs and liposomes.

Nanoparticles were assessed for their toxicity and pro-apoptotic activity on MDA-MB-231 as a breast cancer cell model. The cytotoxicity assessment demonstrated that C6

ceramide-loaded nanoparticles (LNCs-C6 and liposome-C6) were more cytotoxic than the equivalent ghost nanoparticles (LNCs-ghost and liposome-ghost). LNC50s had the highest toxicity, likely because of the surfactant. Importantly, C6-loaded nanoparticles presented similar dose-response profiles compared to free-C6, confirming that the pharmacological activity of the ceramide was maintained.

The ability of C6 ceramide to induce apoptosis was assessed using flow cytometry. The results confirmed that apoptosis *via* caspase-3/7 activation was the main cell death mechanism in MDA-MB-231 cells. Similar to the cytotoxicity results, C6-loaded nanoparticles were more effective in inducing apoptosis than the equivalent ghost nanoparticles. Moreover, LNCs-C6 were slightly more toxic than liposomes-C6.

4.1.3. A good start, but more work is needed on ceramide-loaded LNCs.

Overall, LNCs have been found to be a great potential nanocarrier for ceramide delivery, though further assessment is needed to build on these preliminary results.

4.2. Future Work

This research has provided interesting preliminary data that seems to indicate that LNCs are a suitable alternative nanocarrier for C6 ceramides. In the short-term, the priority should be to assess ceramide loading and release. This work could help confirm whether ceramide exist in the shell of LNCs or are dissolved in the oily core. Following this, uptake studies could be useful to understand better the interaction between LNC-C6 and cancer cells. Additional studies could be performed to provide an in-depth investigation of cellular death mechanism and extend this work to a wider variety of cell models and potentially to additional ceramides. Finally, future work must include testing of drug-loaded ceramide-

containing nanoparticles as a combinatory anticancer treatment. In the longer term, a comprehensive study on cellular or active targeting, such as surface modification using antibodies-, proteins- or peptides-targeted, may be beneficial. This could assist in developing suitable nanocarriers for ceramide delivery directly into tumours, without affecting normal tissue.

5. References

1. Siskind LJ, Mullen TD, Obeid LM. The Role of Ceramide in Cell Regulation. In: Handbook of Cell Signaling, Second Edition. Elsevier; 2009. p. 1201–11.
2. Alonso A, Goñi FM. The Physical Properties of Ceramides in Membranes. Annu Rev Biophys. 2018 May 20;47(1):633–54.
3. Goñi FM, Alonso A. Biophysics of sphingolipids I. Membrane properties of sphingosine, ceramides and other simple sphingolipids. Vol. 1758, Biochimica et Biophysica Acta - Biomembranes. Elsevier; 2006. p. 1902–21.
4. Uchida Y. Ceramide signaling in mammalian epidermis. Vol. 1841, Biochimica et Biophysica Acta - Molecular and Cell Biology of Lipids. 2014. p. 453–62.
5. Coderch L, Lopez O, de la Maza A, Parra JL. Ceramides and Skin Function. Am J Clin Dermatol. 2003;4(2):107–29.
6. Kolesnick RN, Goñi FM, Alonso A. Compartmentalization of Ceramide Signaling: Physical Foundations and Biological Effects. Vol. 184, Journal of Cellular Physiology. 2000. p. 285–300.
7. Hannun YA, Obeid LM. Principles of bioactive lipid signalling: Lessons from sphingolipids. Vol. 9, Nature Reviews Molecular Cell Biology. 2008. p. 139–50.
8. Moro K, Nagahashi M, Gabriel E, Takabe K, Wakai T. Clinical application of ceramide in cancer treatment. Vol. 26, Breast Cancer. Springer Tokyo; 2019. p. 407–15.
9. Watters RJ, Kester M, Tran MA, Loughran TP, Liu X. Development and use of ceramide nanoliposomes in cancer. In: Methods in Enzymology. Academic Press Inc.; 2012. p. 89–108.
10. Sheridan M, Ogretmen B. The role of ceramide metabolism and signaling in the regulation of mitophagy and cancer therapy. Vol. 13, Cancers. MDPI; 2021.
11. Espaillat MP, Shamseddine AA, Adada MM, Hannun YA, Obeid LM. Ceramide and sphingosine-1-phosphate in cancer, two faces of the sphinx. Vol. 4, Translational Cancer Research. AME Publishing Company; 2015. p. 484–99.
12. Radin NS. Killing cancer cells by poly-drug elevation of ceramide levels: A hypothesis whose time has come? Vol. 268, European Journal of Biochemistry. Blackwell Publishing Ltd.; 2001. p. 193–204.
13. Taniguchi M, Okazaki T. The role of sphingomyelin and sphingomyelin synthases in cell death, proliferation and migration - From cell and animal models to human disorders. Vol. 1841, Biochimica et Biophysica Acta - Molecular and Cell Biology of Lipids. Elsevier B.V.; 2014. p. 692–703.
14. Ogretmen B. Sphingolipid metabolism in cancer signalling and therapy. Vol. 18, Nature Reviews Cancer. Nature Publishing Group; 2017. p. 33–50.

15. Ryland LK, Fox TE, Liu X, Loughran TP, Kester M. Dysregulation of sphingolipid metabolism in cancer. Vol. 11, Cancer Biology and Therapy. 2011. p. 138–49.

16. Morad SAF, Levin JC, Shanmugavelandy SS, Kester M, Fabrias G, Bedia C, et al. Ceramide-antiestrogen nanoliposomal combinations-novel impact of hormonal therapy in hormone-insensitive breast cancer. Mol Cancer Ther. 2012 Nov;11(11):2352–61.

17. Taniguchi M, Okazaki T. Role of ceramide/sphingomyelin (SM) balance regulated through “SM cycle” in cancer. Vol. 87, Cellular Signalling. Elsevier Inc.; 2021.

18. Kolesnick RN, Krönke M. Regulation of ceramide production and apoptosis. Vol. 60, Annu. Rev. Physiol. 1998.

19. Noda S, Yoshimura SI, Sawada M, Naganawa T, Iwama T, Nakashima S, et al. Role of ceramide during cisplatin-induced apoptosis in C6 glioma cells. Vol. 52, Journal of Neuro-Oncology. 2001.

20. Olshefski RS, Ladisch S. Glucosylceramide synthase inhibition enhances vincristine-induced cytotoxicity. Int J Cancer. 2001 Jul 1;93(1):131–8.

21. Liu YY, Yu JY, Yin D, Patwardhan GA, Gupta V, Hirabayashi Y, et al. A role for ceramide in driving cancer cell resistance to doxorubicin. The FASEB Journal. 2008 Jul;22(7):2541–51.

22. Grösch S, Schiffmann S, Geisslinger G. Chain length-specific properties of ceramides. Vol. 51, Progress in Lipid Research. 2012. p. 50–62.

23. Mullen TD, Hannun YA, Obeid LM. Ceramide synthases at the centre of sphingolipid metabolism and biology. Vol. 441, Biochemical Journal. 2012. p. 789–802.

24. Sot J, Goñi FM, Alonso A. Molecular associations and surface-active properties of short- and long-N-acyl chain ceramides. Biochim Biophys Acta Biomembr. 2005;1711(1):12–9.

25. Fanani ML, Maggio B. The many faces (and phases) of ceramide and sphingomyelin I – single lipids. Vol. 9, Biophysical Reviews. Springer Verlag; 2017. p. 589–600.

26. Ridgway ND, Merriam DL. Metabolism of short-chain ceramide and dihydroceramide analogues in Chinese hamster ovary (CHO) cells. Biochimica et Biophysica Acta (BBA) - Lipids and Lipid Metabolism. 1995 Apr;1256(1):57–70.

27. Park K, Elias PM, Shin KO, Lee YM, Hupe M, Borkowski AW, et al. A Novel Role of a Lipid Species, Sphingosine-1-Phosphate, in Epithelial Innate Immunity. Mol Cell Biol. 2013 Feb 1;33(4):752–62.

28. Sultan I, Senkal CE, Ponnusamy S, Bielawski J, Szulc Z, Bielawska A, et al. Regulation of the sphingosine-recycling pathway for ceramide generation by oxidative stress, and its role in controlling c-Myc/Max function. Biochemical Journal. 2006 Jan 15;393(2):513–21.

29. Ghosh S, Juin SK, Nandi P, Majumdar SB, Bose A, Baral R, et al. PKCζ mediated anti-proliferative effect of C2 ceramide on neutralization of the tumor microenvironment and melanoma regression. Cancer Immunology, Immunotherapy. 2020 Apr 1;69(4):611–27.

30. Tan KB, Ling LU, Bunte RM, Chng WJ, Chiu GNC. Liposomal codelivery of a synergistic combination of bioactive lipids in the treatment of acute myeloid leukemia. Nanomedicine. 2014 Aug 1;9(11):1665–79.

31. Stover T, Kester M. Liposomal Delivery Enhances Short-Chain Ceramide-Induced Apoptosis of Breast Cancer Cells. Journal of Pharmacology and Experimental Therapeutics. 2003 Nov;307(2):468–75.

32. Stover TC, Sharma A, Robertson GP, Kester M. Systemic Delivery of Liposomal Short-Chain Ceramide Limits Solid Tumor Growth in Murine Models of Breast Adenocarcinoma. Clinical Cancer Research. 2005 May 1;11(9):3465–74.

33. Shabbits JA, Mayer LD. Intracellular delivery of ceramide lipids via liposomes enhances apoptosis in vitro. Biochim Biophys Acta Biomembr. 2003 May 2;1612(1):98–106.

34. Flowers M, Fabriás G, Delgado A, Casas J, Abad JL, Cabot MC. C6-Ceramide and targeted inhibition of acid ceramidase induce synergistic decreases in breast cancer cell growth. Breast Cancer Res Treat. 2012 Jun;133(2):447–58.

35. Fonseca NA, Gomes-Da-Silva LC, Moura V, Simões S, Moreira JN. Simultaneous active intracellular delivery of doxorubicin and C6-ceramide shifts the additive/antagonistic drug interaction of non-encapsulated combination. Journal of Controlled Release. 2014 Dec 28;196:122–31.

36. Sriraman SK, Pan J, Sarisozen C, Luther E, Torchilin V. Enhanced Cytotoxicity of Folic Acid-Targeted Liposomes Co-Loaded with C6 Ceramide and Doxorubicin: In Vitro Evaluation on HeLa, A2780-ADR, and H69-AR Cells. Mol Pharm. 2016 Feb 1;13(2):428–37.

37. Chen M Bin, Jiang Q, Liu Y yuan, Zhang Y, He B shun, Wei MX, et al. C6 ceramide dramatically increases vincristine sensitivity both in vivo and in vitro, involving AMP-activated protein kinase-p53 signaling. Carcinogenesis. 2015 Mar 24;36(9):1061–70.

38. Jiang Y, DiVittore NA, Kaiser JM, Shanmugavelandy SS, Fritz JL, Heakal Y, et al. Combinatorial therapies improve the therapeutic efficacy of nanoliposomal ceramide for pancreatic cancer. Cancer Biol Ther. 2011 Oct 1;12(7):574–85.

39. Zhao X, Sun B, Zhang J, Zhang R, Zhang Q. Short-chain C6 ceramide sensitizes AT406-induced anti-pancreatic cancer cell activity. Biochem Biophys Res Commun. 2016 Oct 14;479(2):166–72.

40. Tagaram HRS, DiVittore NA, Barth BM, Kaiser JM, Avella D, Kimchi ET, et al. Nanoliposomal ceramide prevents in vivo growth of hepatocellular carcinoma. Gut. 2011 May;60(5):695–701.

41. Ryland LK, Doshi UA, Shanmugavelandy SS, Fox TE, Aliaga C, Broeg K, et al. C6-ceramide nanoliposomes target the warburg effect in chronic lymphocytic leukemia. PLoS One. 2013 Dec 19;8(12).

42. Su X, Song H, Niu F, Yang K, Kou G, Wang X, et al. Co-delivery of doxorubicin and PEGylated C16-ceramide by nanoliposomes for enhanced therapy against multidrug resistance. Nanomedicine. 2015 Jul 1;10(13):2033–50.

43. Koshkaryev A, Piroyan A, Torchilin VP. Increased apoptosis in cancer cells in vitro and in vivo by ceramides in transferrin-modified liposomes. Cancer Biol Ther. 2012 Jan 1;13(1):50–60.

44. Fillet M, Bentires-Alj M, Deregowski V, Greimers R, Gielen J, Piette J, et al. Mechanisms involved in exogenous C2- and C6-ceramide-induced cancer cell toxicity. Biochem Pharmacol. 2003 May 15;65(10):1633–42.

45. Khazanov E, Priev A, Shillemans JP, Barenholz Y. Physicochemical and biological characterization of ceramide-containing liposomes: Paving the way to ceramide therapeutic application. Langmuir. 2008 Jul 1;24(13):6965–80.

46. Pal P, Atilla-Gokcumen GE, Frasor J. Emerging Roles of Ceramides in Breast Cancer Biology and Therapy. Vol. 23, International Journal of Molecular Sciences. MDPI; 2022.

47. Brovkovych V, Izhar Y, Danes JM, Dubrovskyi O, Sakallioglu IT, Morrow LM, et al. Fatostatin induces pro- and anti-apoptotic lipid accumulation in breast cancer. Oncogenesis. 2018 Aug 1;7(8).

48. Guardiola-Serrano F, Beteta-Göbel R, Rodríguez-Lorca R, Ibarguren M, López DJ, Terés S, et al. The triacylglycerol, hydroxytriolein, inhibits triple negative mammary breast cancer cell proliferation through a mechanism dependent on dihydroceramide and Akt. Vol. 10, Oncotarget. 2019.

49. Øverbye A, Holsaeter AM, Fusser M, Škalko-Basnet N, Iversen TG, Lyngaas Torgersen M, et al. Ceramide-containing liposomes with doxorubicin: time and cell-dependent effect of C6 and C12 ceramide. 2017.

50. Cruz AF, Fonseca NA, Malheiro AR, B. Melo J, Gaspar MM, Fernandes R, et al. Targeted liposomal doxorubicin/ceramides combinations: The importance to assess the nature of drug interaction beyond bulk tumor cells. European Journal of Pharmaceutics and Biopharmaceutics. 2022 Mar 1;172:61–77.

51. Cruz AF, Caleiras MB, Fonseca NA, Gonçalves N, Mendes VM, Sampaio SF, et al. The enhanced efficacy of intracellular delivery of doxorubicin/c6-ceramide combination mediated by the f3 peptide/nucleolin system is supported by the downregulation of the pi3k/akt pathway. Cancers (Basel). 2021 Jun 2;13(12).

52. Lee Y, Na J, Lee MS, Cha EY, Sul JY, Park JB, et al. Combination of pristimerin and paclitaxel additively induces autophagy in human breast cancer cells via ERK1/2 regulation. Mol Med Rep. 2018 Nov 1;18(5):4281–8.

53. Tran MA, Smith CD, Kester M, Robertson GP. Combining nanoliposomal ceramide with sorafenib synergistically inhibits melanoma and breast cancer cell survival to decrease tumor development. Clinical Cancer Research. 2008 Jun 1;14(11):3571–81.

54. Yang L, Zheng LY, Tian Y, Zhang ZQ, Dong WL, Wang XF, et al. C6 ceramide dramatically enhances docetaxel-induced growth inhibition and apoptosis in cultured breast cancer cells: A mechanism study. Exp Cell Res. 2015 Mar 1;332(1):47–59.

55. Liyanage PY, Hettiarachchi SD, Zhou Y, Ouhtit A, Seven ES, Oztan CY, et al. Nanoparticle-mediated targeted drug delivery for breast cancer treatment. Vol. 1871, Biochimica et Biophysica Acta - Reviews on Cancer. Elsevier B.V.; 2019. p. 419–33.

56. Olusanya TOB, Ahmad RRH, Ibegbu DM, Smith JR, Elkordy AA. Liposomal drug delivery systems and anticancer drugs. Vol. 23, Molecules. MDPI AG; 2018.

57. Kester M, Bassler J, Fox TE, Carter CJ, Davidson JA, Parette MR. Preclinical development of a C6-ceramide NanoLiposome, a novel sphingolipid therapeutic. Vol. 396, Biological Chemistry. Walter de Gruyter GmbH; 2015. p. 737–47.

58. Zhang P, Fu C, Hu Y, Dong C, Song Y, Song E. C6-ceramide nanoliposome suppresses tumor metastasis by eliciting PI3K and PKCζ tumor-suppressive activities and regulating integrin affinity modulation. Sci Rep. 2015;5.

59. Haley B, Frenkel E. Nanoparticles for drug delivery in cancer treatment. Vol. 26, Urologic Oncology: Seminars and Original Investigations. 2008. p. 57–64.

60. Yadav D, Sandeep K, Pandey D, Dutta RK. Liposomes for Drug Delivery. J Biotechnol Biomater. 2017;07(04).

61. Liu P, Chen G, Zhang J. A Review of Liposomes as a Drug Delivery System: Current Status of Approved Products, Regulatory Environments, and Future Perspectives. Vol. 27, Molecules. MDPI; 2022.

62. Nel J, Elkhoury K, Velot É, Bianchi A, Acherar S, Francius G, et al. Functionalized liposomes for targeted breast cancer drug delivery. Vol. 24, Bioactive Materials. KeAi Communications Co.; 2023. p. 401–37.

63. Mozafari MR. Liposomes: an overview of manufacturing techniques. Cell Mol Biol Lett. 2005;10(4):711–9.

64. Bhardwaj U, Burgess DJ. Physicochemical properties of extruded and non-extruded liposomes containing the hydrophobic drug dexamethasone. Int J Pharm. 2010 Mar 30;388(1–2):181–9.

65. Hong SS, Kim SH, Lim SJ. Effects of triglycerides on the hydrophobic drug loading capacity of saturated phosphatidylcholine-based liposomes. Int J Pharm. 2015 Apr 15;483(1–2):142–50.

66. Kolter M, Wittmann M, Köll-Weber M, Süss R. The suitability of liposomes for the delivery of hydrophobic drugs – A case study with curcumin. European Journal of Pharmaceutics and Biopharmaceutics. 2019 Jul 1;140:20–8.

67. Sercombe L, Veerati T, Moheimani F, Wu SY, Sood AK, Hua S. Advances and challenges of liposome assisted drug delivery. Vol. 6, Frontiers in Pharmacology. Frontiers Media S.A.; 2015.

68. Zou P, Stern ST, Sun D. PLGA/liposome hybrid nanoparticles for short-chain ceramide delivery. Pharm Res. 2014;31(3):684–93.

69. Wang SB, Ma YY, Chen XY, Zhao YY, Mou XZ. Ceramide-graphene oxide nanoparticles enhance cytotoxicity and decrease HCC xenograft development: A novel approach for targeted cancer therapy. Front Pharmacol. 2019;10(FEB).

70. Adiseshaiah PP, Clogston JD, McLeland CB, Rodriguez J, Potter TM, Neun BW, et al. Synergistic combination therapy with nanoliposomal C6-ceramide and vinblastine is associated with autophagy dysfunction in hepatocarcinoma and colorectal cancer models. Cancer Lett. 2013 Sep 1;337(2):254–65.

71. Huynh NT, Passirani C, Saulnier P, Benoit JP. Lipid nanocapsules: A new platform for nanomedicine. Vol. 379, International Journal of Pharmaceutics. 2009. p. 201–9.

72. Sánchez-Moreno P, Ortega-Vinuesa JL, Martín-Rodríguez A, Boulaiz H, Marchal-Corrales JA, Peula-García JM. Characterization of different functionalized lipidic nanocapsules as potential drug carriers. Int J Mol Sci. 2012 Feb;13(2):2405–24.

73. Heurtault B, Saulnier P, Pech B, Proust JE, Benoit JP. A Novel Phase Inversion-Based Process for the Preparation of Lipid Nanocarriers. 2002.

74. Heurtault B, Saulnier P, Pech B, Venier-Julienne MC, Proust ˆ Jacques-Emile, Phan-Tan-Luu R, et al. The influence of lipid nanocapsule composition on their size distribution. Vol. 18, European Journal of Pharmaceutical Sciences. 2003.

75. Heurtault B, Saulnier P, Pech B, Benoît JP, Proust JE. Interfacial stability of lipid nanocapsules. Colloids Surf B Biointerfaces. 2003 Jul 15;30(3):225–35.

76. Vonarbourg A, Passirani C, Saulnier P, Benoit JP. Parameters influencing the stealthiness of colloidal drug delivery systems. Vol. 27, Biomaterials. 2006. p. 4356–73.

77. Vonarbourg A, Saulnier P, Passirani C, Benoit JP. Electrokinetic properties of noncharged lipid nanocapsules: Influence of the dipolar distribution at the interface. Electrophoresis. 2005 Jun;26(11):2066–75.

78. Lacoeuille F, Garcion E, Benoit JP, Lamprecht A. Lipid nanocapsules for intracellular drug delivery of anticancer drugs. In: Journal of Nanoscience and Nanotechnology. American Scientific Publishers; 2007. p. 4612–7.

79. Garcion E, Lamprecht A, Heurtault B, Paillard A, Aubert-Pouessel A, Denizot B, et al. A new generation of anticancer, drug-loaded, colloidal vectors reverses multidrug resistance in glioma and reduces tumor progression in rats. Mol Cancer Ther. 2006 Jul;5(7):1710–22.

80. Le Roux G, Moche H, Nieto A, Benoit JP, Nesslany F, Lagarce F. Cytotoxicity and genotoxicity of lipid nanocapsules. Toxicology in Vitro. 2017 Jun 1;41:189–99.

81. Maupas C, Moulari B, Béduneau A, Lamprecht A, Pellequer Y. Surfactant dependent toxicity of lipid nanocapsules in HaCaT cells. Int J Pharm. 2011 Jun 15;411(1–2):136–41.

82. Manaargadoo-Catin M, Ali-Cherif A, Pougnas JL, Perrin C. Hemolysis by surfactants - A review. Vol. 228, Advances in Colloid and Interface Science. Elsevier; 2016. p. 1–16.

83. BASF. Kolliphor® HS15 Technical Information. 2020.

84. Liu L, Mao K, Wang W, Pan H, Wang F, Yang M, et al. Kolliphor® HS 15 Micelles for the Delivery of Coenzyme Q10: Preparation, Characterization, and Stability. AAPS PharmSciTech. 2016 Jun 1;17(3):757–66.

85. Séguy L, Groo AC, Goux D, Hennequin D, Malzert-Fréon A. Design of non-haemolytic nanoemulsions for intravenous administration of hydrophobic APIs. Pharmaceutics. 2020 Dec 1;12(12):1–20.

86. Basu SM, Yadava SK, Singh R, Giri J. Lipid nanocapsules co-encapsulating paclitaxel and salinomycin for eradicating breast cancer and cancer stem cells. Colloids Surf B Biointerfaces. 2021 Aug 1;204.

87. El-Sheridy NA, El-Moslemany RM, Ramadan AA, Helmy MW, El-Khordagui LK. Enhancing the in vitro and in vivo activity of itraconazole against breast cancer using miltefosine-modified lipid nanocapsules. Drug Deliv. 2021;28(1):906–19.

88. Idlas P, Lepeltier E, Bastiat G, Pigeon P, McGlinchey MJ, Lautram N, et al. Physicochemical Characterization of Ferrocifen Lipid Nanocapsules: Customized Drug Delivery Systems Guided by the Molecular Structure. Langmuir. 2023 Feb 7;39(5):1885–96.

89. Idlas P, Lepeltier E, Jaouen G, Passirani C. Ferrocifen loaded lipid nanocapsules: A promising anticancer medication against multidrug resistant tumors. Vol. 13, Cancers. MDPI; 2021.

90. Radwan Y, Arafa KK, Ghoniem MG, Al-Farraj ES, El-Sherbiny IM. An in-vitro quantitative investigation on the synergistic effect of capsaicin and 5-fluorouracil encapsulated into lipid nanocapsules to treat breast cancer. Drug Dev Ind Pharm. 2023;

91. Morad SAF, Cabot MC. Ceramide-orchestrated signalling in cancer cells. Vol. 13, Nature Reviews Cancer. 2013. p. 51–65.

92. Migotto A, Carvalho VFM, Salata GC, da Silva FWM, Yan CYI, Ishida K, et al. Multifunctional nanoemulsions for intraductal delivery as a new platform for local treatment of breast cancer. Drug Deliv. 2018;25(1):654–67.

93. Carvalho VFM, Migotto A, Giacone D V., de Lemos DP, Zanoni TB, Maria-Engler SS, et al. Co-encapsulation of paclitaxel and C6 ceramide in tributyrin-containing nanocarriers improve co-localization in the skin and potentiate cytotoxic effects in 2D and 3D models. European Journal of Pharmaceutical Sciences. 2017 Nov 15;109:131–43.

94. Deshpande D, Janero DR, Amiji M. Engineering of an ω-3 polyunsaturated fatty acid-containing nanoemulsion system for combination C6-ceramide and 17β-estradiol delivery and bioactivity in human vascular endothelial and smooth muscle cells. Nanomedicine. 2013 Oct;9(7):885–94.

95. Balakrishnan P, Song CK, Jahn A, Cho HJ. Ceramide and N,N,N-Trimethylphytosphingosine-Iodide (TMP-I)-Based Lipid Nanoparticles for Cancer Therapy. Pharm Res. 2016 Jan 1;33(1):206–16.

96. Raval N, Maheshwari R, Kalyane D, Youngren-Ortiz SR, Chougule MB, Tekade RK. Importance of physicochemical characterization of nanoparticles in pharmaceutical product development. In: Basic Fundamentals of Drug Delivery. Elsevier; 2018. p. 369–400.

97. Zhang S, Li J, Lykotrafitis G, Bao G, Suresh S. Size-dependent endocytosis of nanoparticles. Advanced Materials. 2009 Jan 26;21(4):419–24.

98. Mills JA, Liu F, Jarrett TR, Fletcher NL, Thurecht KJ. Nanoparticle based medicines: approaches for evading and manipulating the mononuclear phagocyte system and potential for clinical translation. Vol. 10, Biomaterials Science. Royal Society of Chemistry; 2022. p. 3029–53.

99. Alexis F, Pridgen E, Molnar LK, Farokhzad OC. Factors affecting the clearance and biodistribution of polymeric nanoparticles. In: Molecular Pharmaceutics. 2008. p. 505–15.

100. Wei D, Pang K, Song Q, Suo Y, He H, Weng X, et al. Noninvasive monitoring of nanoparticle clearance and aggregation in blood circulation by in vivo flow cytometry. Journal of Controlled Release. 2018 May 28;278:66–73.

101. Mills JA, Humphries J, Simpson JD, Sonderegger SE, Thurecht KJ, Fletcher NL. Modulating Macrophage Clearance of Nanoparticles: Comparison of Small-Molecule and Biologic Drugs as Pharmacokinetic Modifiers of Soft Nanomaterials. Mol Pharm. 2022 Nov 7;19(11):4080–97.

102. Shang L, Nienhaus K, Nienhaus GU. Engineered nanoparticles interacting with cells: Size matters. Vol. 12, Journal of Nanobiotechnology. 2014.

103. Kumar A, Dixit CK. Methods for characterization of nanoparticles. In: Advances in Nanomedicine for the Delivery of Therapeutic Nucleic Acids. Elsevier Inc.; 2017. p. 44–58.

104. Hoo CM, Starostin N, West P, Mecartney ML. A comparison of atomic force microscopy (AFM) and dynamic light scattering (DLS) methods to characterize nanoparticle size distributions. Journal of Nanoparticle Research. 2008 Dec;10(SUPPL. 1):89–96.

105. Danaei M, Dehghankhold M, Ataei S, Hasanzadeh Davarani F, Javanmard R, Dokhani A, et al. Impact of particle size and polydispersity index on the clinical applications of lipidic nanocarrier systems. Vol. 10, Pharmaceutics. MDPI AG; 2018.

106. Bhatia S. Nanoparticles Types, Classification, Characterization, Fabrication Methods and Drug Delivery Applications. Natural Polymer Drug Delivery Systems: Nanoparticles, Plants, and Algae. Cham: Springer International Publishing; 2016. p. 33–93.

107. Xu R. Progress in nanoparticles characterization: Sizing and zeta potential measurement. Particuology. 2008 Apr;6(2):112–5.

108. Mitchell MJ, Billingsley MM, Haley RM, Wechsler ME, Peppas NA, Langer R. Engineering precision nanoparticles for drug delivery. Vol. 20, Nature Reviews Drug Discovery. Nature Research; 2021. p. 101–24.

109. Ernst LM, Casals E, Italiani P, Boraschi D, Puntes V. The interactions between nanoparticles and the innate immune system from a nanotechnologist perspective. Vol. 11, Nanomaterials. MDPI; 2021.

110. Ray P, Haideri N, Haque I, Mohammed O, Chakraborty S, Banerjee S, et al. The Impact of Nanoparticles on the Immune System: A Gray Zone of Nanomedicine. Vol. 5, Journal of Immunological Sciences Review Article. 2021.

111. Chen L, Liu J, Zhang Y, Zhang G, Kang Y, Chen A, et al. The toxicity of silica nanoparticles to the immune system. Vol. 13, Nanomedicine. Future Medicine Ltd.; 2018. p. 1939–62.

112. Liu Y, Hardie J, Zhang X, Rotello VM. Effects of engineered nanoparticles on the innate immune system. Vol. 34, Seminars in Immunology. Academic Press; 2017. p. 25–32.

113. Xiao Y, Wiesner MR. Characterization of surface hydrophobicity of engineered nanoparticles. J Hazard Mater. 2012 May 15;215–216:146–51.

114. Acosta E. Bioavailability of nanoparticles in nutrient and nutraceutical delivery. Vol. 14, Current Opinion in Colloid and Interface Science. 2009. p. 3–15.

115. Cölfen H. Double-hydrophilic block copolymers: Synthesis and application as novel surfactants and crystal growth modifiers. Vol. 22, Macromolecular Rapid Communications. 2001. p. 219–52.

116. Madenci D, Egelhaaf SU. Self-assembly in aqueous bile salt solutions. Vol. 15, Current Opinion in Colloid and Interface Science. 2010. p. 109–15.

117. Jones MC, Jones SA, Riffo-Vasquez Y, Spina D, Hoffman E, Morgan A, et al. Quantitative assessment of nanoparticle surface hydrophobicity and its influence on pulmonary biocompatibility. Journal of Controlled Release. 2014 Jun 10;183(1):94–104.

118. Handy RD, Owen R, Valsami-Jones E. The ecotoxicology of nanoparticles and nanomaterials: Current status, knowledge gaps, challenges, and future needs. Vol. 17, Ecotoxicology. 2008. p. 315–25.

119. Verma A, Uzun O, Hu Y, Hu Y, Han HS, Watson N, et al. Surface-structure-regulated cell-membrane penetration by monolayer-protected nanoparticles. Nat Mater. 2008;7(7):588–95.

120. Saptarshi SR, Duschl A, Lopata AL. Interaction of nanoparticles with proteins: Relation to bio-reactivity of the nanoparticle. J Nanobiotechnology. 2013 Jul 19;11(1).

121. Gessner A, Waicz R, Lieske A, Paulke BR, Mäder K, Müller RH. Nanoparticles with decreasing surface hydrophobicities: influence on plasma protein adsorption. Int J Pharm. 2000 Mar;196(2):245–9.

122. Sharma A, Madhunapantula S V., Robertson GP. Toxicological considerations when creating nanoparticle-based drugs and drug delivery systems. Vol. 8, Expert Opinion on Drug Metabolism and Toxicology. 2012. p. 47–69.

123. Ljungh A, Hjertén S, Wadström T. High surface hydrophobicity of autoaggregating Staphylococcus aureus strains isolated from human infections studied with the salt aggregation test. Infect Immun. 1985 Feb;47(2):522–6.

124. Sadeghi R, Jahani F. Salting-in and salting-out of water-soluble polymers in aqueous salt solutions. Journal of Physical Chemistry B. 2012 May 3;116(17):5234–41.

125. Vonarbourg A, Passirani C, Saulnier P, Simard P, Leroux JC, Benoit JP. Evaluation of pegylated lipid nanocapsules versus complement system activation and macrophage uptake. J Biomed Mater Res A. 2006 Sep 1;78(3):620–8.

126. Szwed M, Torgersen ML, Kumari RV, Yadava SK, Pust S, Iversen TG, et al. Biological response and cytotoxicity induced by lipid nanocapsules. J Nanobiotechnology. 2020 Jan 6;18(1).

127. Dulieu C, Bazile D. Influence of lipid nanocapsules composition on their aptness to freeze-drying. Pharm Res. 2005 Feb;22(2):285–92.

128. Anderson M, Omri A. The Effect of Different Lipid Components on the in Vitro Stability and Release Kinetics of Liposome Formulations. Drug Delivery: Journal of Delivery and Targeting of Therapeutic Agents. 2004 Jan;11(1):33–9.

129. Pietzyk B, Henschke K. Degradation of phosphatidylcholine in liposomes containing carboplatin in dependence on composition and storage conditions. Int J Pharm. 2000 Mar;196(2):215–8.

130. Hashemzadeh H, Javadi H, Darvishi MH. Study of Structural stability and formation mechanisms in DSPC and DPSM liposomes: A coarse-grained molecular dynamics simulation. Sci Rep. 2020 Dec 1;10(1).

131. Balgavý P, Dubničková M, Kučerka N, Kiselev MA, Yaradaikin SP, Uhríková D. Bilayer thickness and lipid interface area in unilamellar extruded 1,2-diacylphosphatidylcholine liposomes: a small-angle neutron scattering study. Biochimica et Biophysica Acta (BBA) - Biomembranes. 2001 May;1512(1):40–52.

132. Drabik D, Chodaczek G, Kraszewski S, Langner M. Mechanical Properties Determination of DMPC, DPPC, DSPC, and HSPC Solid-Ordered Bilayers. Langmuir. 2020 Apr 14;36(14):3826–35.

133. Zolnik BS, Stern ST, Kaiser JM, Heakal Y, Clogston JD, Kester M, et al. Rapid distribution of liposomal short-chain ceramide in vitro and in vivo. Drug Metabolism and Disposition. 2008 Aug;36(8):1709–15.

134. Nakhaei P, Margiana R, Bokov DO, Abdelbasset WK, Jadidi Kouhbanani MA, Varma RS, et al. Liposomes: Structure, Biomedical Applications, and Stability Parameters With Emphasis on Cholesterol. Vol. 9, Frontiers in Bioengineering and Biotechnology. Frontiers Media S.A.; 2021.

135. Subczynski WK, Pasenkiewicz-Gierula M, Widomska J, Mainali L, Raguz M. High Cholesterol/Low Cholesterol: Effects in Biological Membranes: A Review. Cell Biochem Biophys. 2017 Dec 1;75(3–4):369–85.

136. Maxfield FR, Tabas I. Role of cholesterol and lipid organization in disease. Nature. 2005 Dec 1;438(7068):612–21.

137. Liu Z, Fu R, Yuying Y. Preparation and evaluation of stable nanofluids for heat transfer application. In: Advances in Nanofluid Heat Transfer. Elsevier; 2022. p. 25–57.

138. Israelachvili JN. Intermolecular and Surface Forces. Third. Vol. Chapter 20. 1992.

139. Megha, Sawatzki P, Kolter T, Bittman R, London E. Effect of ceramide N-acyl chain and polar headgroup structure on the properties of ordered lipid domains (lipid rafts). Biochim Biophys Acta Biomembr. 2007 Sep;1768(9):2205–12.

140. Nybond S, Björkqvist YJE, Ramstedt B, Slotte JP. Acyl chain length affects ceramide action on sterol/sphingomyelin-rich domains. Biochim Biophys Acta Biomembr. 2005 Dec 1;1718(1–2):61–6.

141. Ljungh Å, Wadström T. Salt aggregation test for measuring cell surface hydrophobicity of urinaryEscherichia coli. Eur J Clin Microbiol. 1982 Dec;1(6):388–93.

142. Lindahl M, Faris A, Wadström T, Hjertén S. A new test based on 'salting out' to measure relative hydrophobicity of bacterial cells. Biochimica et Biophysica Acta (BBA) - General Subjects. 1981 Nov;677(3–4):471–6.

143. Santander-Ortega MJ, Csaba N, Alonso MJ, Ortega-Vinuesa JL, Bastos-González D. Stability and physicochemical characteristics of PLGA, PLGA:poloxamer and PLGA:poloxamine blend nanoparticles. A comparative study. Colloids Surf A Physicochem Eng Asp. 2007 Mar 15;296(1–3):132–40.

144. Doran PM. Unit Operations. In: Bioprocess Engineering Principles. Second Edition. Elsevier; 2013. p. 445–595.

145. Li M, Jiang S, Simon J, Paßlick D, Frey ML, Wagner M, et al. Brush conformation of polyethylene glycol determines the stealth effect of nanocarriers in the low protein adsorption regime. Nano Lett. 2021 Feb 24;21(4):1591–8.

146. Kanamaru T, Sakurai K, Fujii S. Impact of Polyethylene Glycol (PEG) Conformations on the in Vivo Fate and Drug Release Behavior of PEGylated Core-Cross-Linked Polymeric Nanoparticles. Biomacromolecules. 2022 Sep 12;23(9):3909–18.

147. Lebreton V, Legeay S, Vasylaki A, Lagarce F, Saulnier P. Protein corona formation on lipidic nanocapsules: Influence of the interfacial PEG repartition. European Journal of Pharmaceutical Sciences. 2023 Oct 1;189.

148. Tirosh O, Barenholz Y, Katzhendler J, Priev A. Hydration of polyethylene glycol-grafted liposomes. Biophys J. 1998;74(3):1371–9.

149. Needham D, Mclatosh TJ, Lasic DD. Repulsive interactions and mechanical stability of polymer-grafted lipid membranes. Vol. 1108, Biochimiea el Biophysica Acta. 1992.

150. Holliday DL, Speirs V. Choosing the right cell line for breast cancer research. Breast Cancer Research. 2011;13(4):215.

151. Chavez KJ, Garimella S V., Lipkowitz S. Triple negative breast cancer cell lines: One tool in the search for better treatment of triple negative breast cancer. Breast Dis. 2010;32(1–2):35–48.

152. Azizi M, Ghourchian H, Yazdian F, Dashtestani F, AlizadehZeinabad H. Cytotoxic effect of albumin coated copper nanoparticle on human breast cancer cells of MDA-MB 231. PLoS One. 2017 Nov 1;12(11).

153. Dong Y, Liao H, Yu J, Fu H, Zhao D, Gong K, et al. Incorporation of drug efflux inhibitor and chemotherapeutic agent into an inorganic/organic platform for the effective treatment of multidrug resistant breast cancer. J Nanobiotechnology. 2019 Dec 23;17(1).

154. Huang Q, Cai T, Bai L, Huang Y, Li Q, Wang Q, et al. State of the art of overcoming efflux transporter mediated multidrug resistance of breast cancer. Vol. 8, Translational Cancer Research. AME Publishing Company; 2019. p. 319–29.

155. Johnson ZL, Chen J. Structural Basis of Substrate Recognition by the Multidrug Resistance Protein MRP1. Cell. 2017 Mar 9;168(6):1075-1085.e9.

156. Taylor NMI, Manolaridis I, Jackson SM, Kowal J, Stahlberg H, Locher KP. Structure of the human multidrug transporter ABCG2. Nature. 2017 Jun 22;546(7659):504–9.

157. Kong JN, He Q, Wang G, Dasgupta S, Dinkins MB, Zhu G, et al. Guggulsterone and bexarotene induce secretion of exosome-associated breast cancer resistance protein and reduce doxorubicin resistance in MDA-MB-231 cells. Int J Cancer. 2015 Oct 1;137(7):1610–20.

158. Cai L, Qin X, Xu Z, Song Y, Jiang H, Wu Y, et al. Comparison of Cytotoxicity Evaluation of Anticancer Drugs between Real-Time Cell Analysis and CCK-8 Method. ACS Omega. 2019 Jul 31;4(7):12036–42.

159. Präbst K, Engelhardt H, Ringgeler S, Hübner H. Basic Colorimetric Proliferation Assays: MTT, WST, and Resazurin. In 2017. p. 1–17.

160. Aslantürk ÖS. In Vitro Cytotoxicity and Cell Viability Assays: Principles, Advantages, and Disadvantages. In: Genotoxicity - A Predictable Risk to Our Actual World. InTech; 2018.

161. Jiao G, He X, Li X, Qiu J, Xu H, Zhang N, et al. Limitations of MTT and CCK-8 assay for evaluation of graphene cytotoxicity. RSC Adv. 2015;5(66):53240–4.

162. Segawa K, Nagata S. An Apoptotic 'Eat Me' Signal: Phosphatidylserine Exposure. Vol. 25, Trends in Cell Biology. Elsevier Ltd; 2015. p. 639–50.

163. Fink SL, Cookson BT. Apoptosis, pyroptosis, and necrosis: Mechanistic description of dead and dying eukaryotic cells. Vol. 73, Infection and Immunity. 2005. p. 1907–16.

164. Crowley LC, Marfell BJ, Scott AP, Boughaba JA, Chojnowski G, Christensen ME, et al. Dead cert: Measuring cell death. Cold Spring Harb Protoc. 2016 Dec 1;2016(12):1064–72.

165. Elmore S. Apoptosis: A Review of Programmed Cell Death. Toxicol Pathol. 2007 Jun 25;35(4):495–516.

166. Shlomovitz I, Speir M, Gerlic M. Flipping the dogma - Phosphatidylserine in non-apoptotic cell death. Vol. 17, Cell Communication and Signaling. BioMed Central Ltd.; 2019.

167. Vermes I, Haanen C, Steffens-Nakken H, Reutellingsperger C. A novel assay for apoptosis Flow cytometric detection of phosphatidylserine expression on early apoptotic cells using fluorescein labelled Annexin V. J Immunol Methods. 1995 Jul;184(1):39–51.

168. Liu ZG, Jiao D. Necroptosis, tumor necrosis and tumorigenesis. Cell Stress. 2020 Jan 1;4(1):1–8.

169. Ferraro-Peyret C, Quemeneur L, Flacher M, Revillard JP, Genestier L. Caspase-Independent Phosphatidylserine Exposure During Apoptosis of Primary T Lymphocytes. The Journal of Immunology. 2002 Nov 1;169(9):4805–10.

170. Balderstone LA, Dawson JC, Welman A, Serrels A, Wedge SR, Brunton VG. Development of a fluorescence-based cellular apoptosis reporter. Methods Appl Fluoresc. 2019;7(1).

171. Baliga BC, Read SH, Kumar S. The biochemical mechanism of caspase-2 activation. Cell Death Differ. 2004 Nov;11(11):1234–41.

172. Kumar S. Caspase function in programmed cell death. Vol. 14, Cell Death and Differentiation. 2007. p. 32–43.

173. Galluzzi L, Vitale I, Aaronson SA, Abrams JM, Adam D, Agostinis P, et al. Molecular mechanisms of cell death: Recommendations of the Nomenclature Committee on Cell Death 2018. Vol. 25, Cell Death and Differentiation. Nature Publishing Group; 2018. p. 486–541.

174. Shi Y. Mechanisms of caspase activation and inhibition during apoptosis. Vol. 9, Molecular Cell. Cell Press; 2002. p. 459–70.

175. Lakhani SA, Masud A, Kuida K, Porter GA, Booth CJ, Mehal WZ, et al. Caspases 3 and 7: Key mediators of mitochondrial events of apoptosis. Science (1979). 2006 Feb 10;311(5762):847–51.

176. Brentnall M, Rodriguez-Menocal L, De Guevara RL, Cepero E, Boise LH. Caspase-9, caspase-3 and caspase-7 have distinct roles during intrinsic apoptosis. BMC Cell Biol. 2013 Jul 9;14(1).

177. Parrish AB, Freel CD, Kornbluth S. Cellular mechanisms controlling caspase activation and function. Cold Spring Harb Perspect Biol. 2013 Jun;5(6).

178. Mohammed Siddiq A, Thangam R, Madhan B, Alam MS. Green (gemini) surfactant mediated gold nanoparticles green synthesis: Effect on triple negative breast cancer cells. Nano-Structures and Nano-Objects. 2019 Jul 1;19.

179. Schöler N, Olbrich C, Tabatt K, Müller RH, Hahn H, Liesenfeld O. Surfactant, but not the size of solid lipid nanoparticles (SLN) influences viability and cytokine production of macrophages. Int J Pharm. 2001 Jun;221(1–2):57–67.

180. Mohammadinejad R, Moosavi MA, Tavakol S, Vardar DÖ, Hosseini A, Rahmati M, et al. Necrotic, apoptotic and autophagic cell fates triggered by nanoparticles. Vol. 15, Autophagy. Taylor and Francis Inc.; 2019. p. 4–33.

181. Wang S, Chen Y, Guo J, Huang Q. Liposomes for Tumor Targeted Therapy: A Review. Vol. 24, International Journal of Molecular Sciences. MDPI; 2023.

182. Chowdhury N, Chaudhry S, Hall N, Olverson G, Zhang QJ, Mandal T, et al. Targeted Delivery of Doxorubicin Liposomes for Her-2+ Breast Cancer Treatment. AAPS PharmSciTech. 2020 Aug 1;21(6).

183. Paillard A, Hindré F, Vignes-Colombeix C, Benoit JP, Garcion E. The importance of endo-lysosomal escape with lipid nanocapsules for drug subcellular bioavailability. Biomaterials. 2010;31(29):7542–54.

184. Moosavi MA, Sharifi M, Ghafary SM, Mohammadalipour Z, Khataee A, Rahmati M, et al. Photodynamic N-TiO2 nanoparticle treatment induces controlled ROS-mediated autophagy and terminal differentiation of leukemia cells. Sci Rep. 2016 Oct 4;6.

185. Davis ME, Chen Z, Shin DM. Nanoparticle therapeutics: an emerging treatment modality for cancer. Nat Rev Drug Discov. 2008 Sep;7(9):771–82.

186. Choi MK, Song IS. Recent advances in the formulation of sphingolipid anticancer therapeutics. Vol. 50, Journal of Pharmaceutical Investigation. Springer; 2020. p. 295–307.

187. Nel M, Joubert AM, Dohle W, Potter BVL, Theron AE. Modes of cell death induced by tetrahydroisoquinoline-based analogs in MDA-MB-231 breast and A549 lung cancer cell lines. Drug Des Devel Ther. 2018 Jun 25;12:1881–904.

188. Mariño G, Kroemer G. Mechanisms of apoptotic phosphatidylserine exposure. Vol. 23, Cell Research. 2013. p. 1247–8.

189. Vermes I, Haanen C, Reutelingsperger C. Flow cytometry of apoptotic cell death. Vol. 243, Journal of Immunological Methods. 2000.

190. Ali-Boucetta H, Al-Jamal KT, Müller KH, Li S, Porter AE, Eddaoudi A, et al. Cellular uptake and cytotoxic impact of chemically functionalized and polymer-coated carbon nanotubes. Small. 2011 Nov 18;7(22):3230–8.

191. Walker JM. Methods in molecular biology™ Series Editor [Internet]. Available from: http://www.springer.com/series/7651

192. Suganya USU, Govindaraju K, Kumar GG, Prabhu D, Arulvasu C, Dhas SS, et al. Anti-proliferative effect of biogenic gold nanoparticles against breast cancer cell lines (MDA-MB-231 & MCF-7). Appl Surf Sci. 2016 May 15;371:415–24.

193. Cavanagh RJ, Smith PA, Stolnik S. Exposure to a Nonionic Surfactant Induces a Response Akin to Heat-Shock Apoptosis in Intestinal Epithelial Cells: Implications for Excipients Safety. Mol Pharm. 2019 Feb 4;16(2):618–31.

194. Kupcho K, Shultz J, Hurst R, Hartnett J, Zhou W, Machleidt T, et al. A real-time, bioluminescent annexin V assay for the assessment of apoptosis. Apoptosis. 2019 Feb 15;24(1–2):184–97.

195. Nguyen QD, Smith G, Glaser M, Perumal M, Årstad E, Aboagye EO. Positron emission tomography imaging of drug-induced tumor apoptosis with a caspase-3/7 specific [18F]-labeled isatin sulfonamide. Proc Natl Acad Sci U S A. 2009 Sep 22;106(38):16375–80.

196. Huerta S, Goulet EJ, Huerta-Yepez S, Livingston EH. Screening and Detection of Apoptosis. Vol. 139, Journal of Surgical Research. 2007. p. 143–56.

197. Shim MK, Yoon HY, Lee S, Jo MK, Park J, Kim JH, et al. Caspase-3/-7-Specific Metabolic Precursor for Bioorthogonal Tracking of Tumor Apoptosis. Sci Rep. 2017 Dec 1;7(1).

198. Cen H, Mao F, Aronchik I, Fuentes RJ, Firestone GL. DEVD-NucView488: a novel class of enzyme substrates for real-time detection of caspase-3 activity in live cells. The FASEB Journal. 2008 Jul;22(7):2243–52.

199. Di Paola M, Cocco T, Lorusso M. Ceramide interaction with the respiratory chain of heart mitochondria. Biochemistry. 2000 Jun 6;39(22):6660–8.

200. Hearps AC, Burrows J, Connor CE, Woods GM, Lowenthal RM, Ragg SJ. Mitochondrial cytochrome c release precedes transmembrane depolarisation and caspase-3 activation during ceramide-induced apoptosis of Jurkat T cells. Vol. 7, Apoptosis. Kluwer Academic Publishers; 2002.

6. Supplementary Information

6.1. Calibration curve for excess surfactant assay

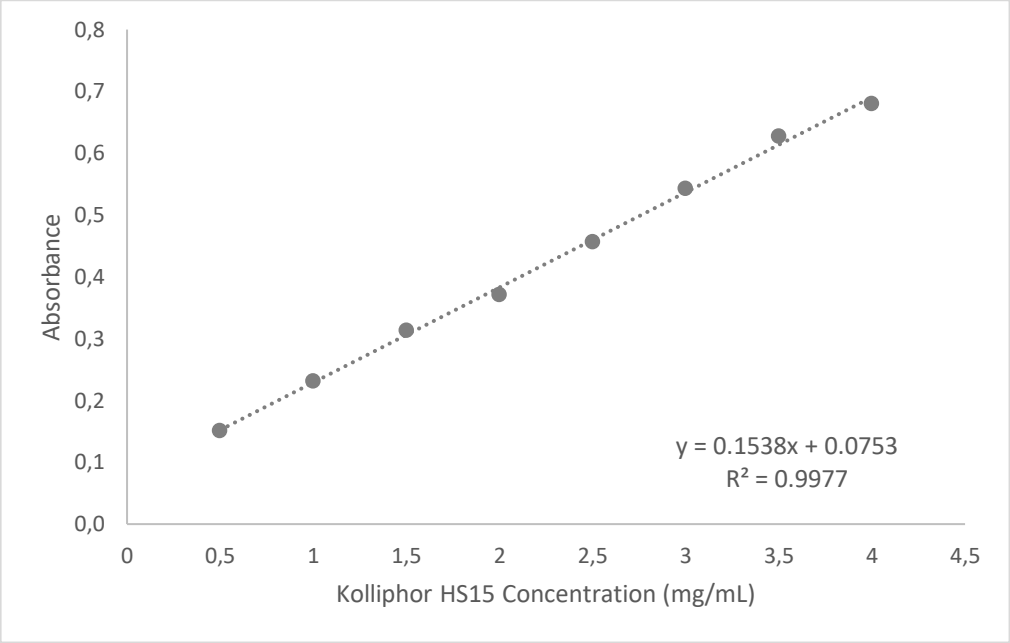

Figure S1. Calibration curve for quantification of excess surfactant (Kolliphor® HS15)

6.2. Validation method of residual surfactant assay (Kolliphor® HS 15)

Conc (mg/mL)	Absorbance			Average Absorbance (Y)	True Absorbance (Yi)	Y-Yi	$(Y-Yi)^2$
	I	II	III				
0.5	0.145	0.141	0.167	0.150666667	0.152202778	-0.001536111	2.35964E-06
1	0.233	0.229	0.231	0.2309	0.229109127	0.001790873	3.20723E-06
1.5	0.318	0.314	0.307	0.312933333	0.306015476	0.006917857	4.78567E-05
2	0.353	0.380	0.379	0.370433333	0.382921825	-0.012488492	0.000155962
2.5	0.464	0.462	0.443	0.456433333	0.459828175	-0.003394841	1.15249E-05
3	0.553	0.531	0.544	0.5427	0.536734524	0.005965476	3.55869E-05
3.5	0.625	0.630	0.626	0.627266667	0.613640873	0.013625794	0.000185662
4	0.683	0.676	0.680	0.679666667	0.690547222	-0.010880556	0.000118386
						Σ	0.000560547
						Σ/(n-2)	9.34244E-05
						σ	0.009665632

where,

Σ = sums of $(Y-Yi)^2$

n = number of samples

σ = standard deviation of absorbances (square root of $(\Sigma/(n-2))$

$$\text{Limit of detection (LoD)} = \frac{3.3 \text{ x } \sigma}{\text{slope of calibration curve}} = \frac{3.3 \text{ x } 0.009665632}{0.1538} = 0.21 \text{ mg/mL}$$

$$\text{Limit of quantification (LoQ)} = \frac{10 \text{ x } \sigma}{\text{slope of calibration curve}} = \frac{10 \text{ x } 0.009665632}{0.1538} = 0.63 \text{ mg/mL}$$

6.3. Flow cytometric analysis of caspase-3/7 activity assay

The quadrant suggested live cells (lower left quadrant/ Q4), apoptotic cells (lower right/ Q3), and dead cells (upper right quadrant/ Q2).

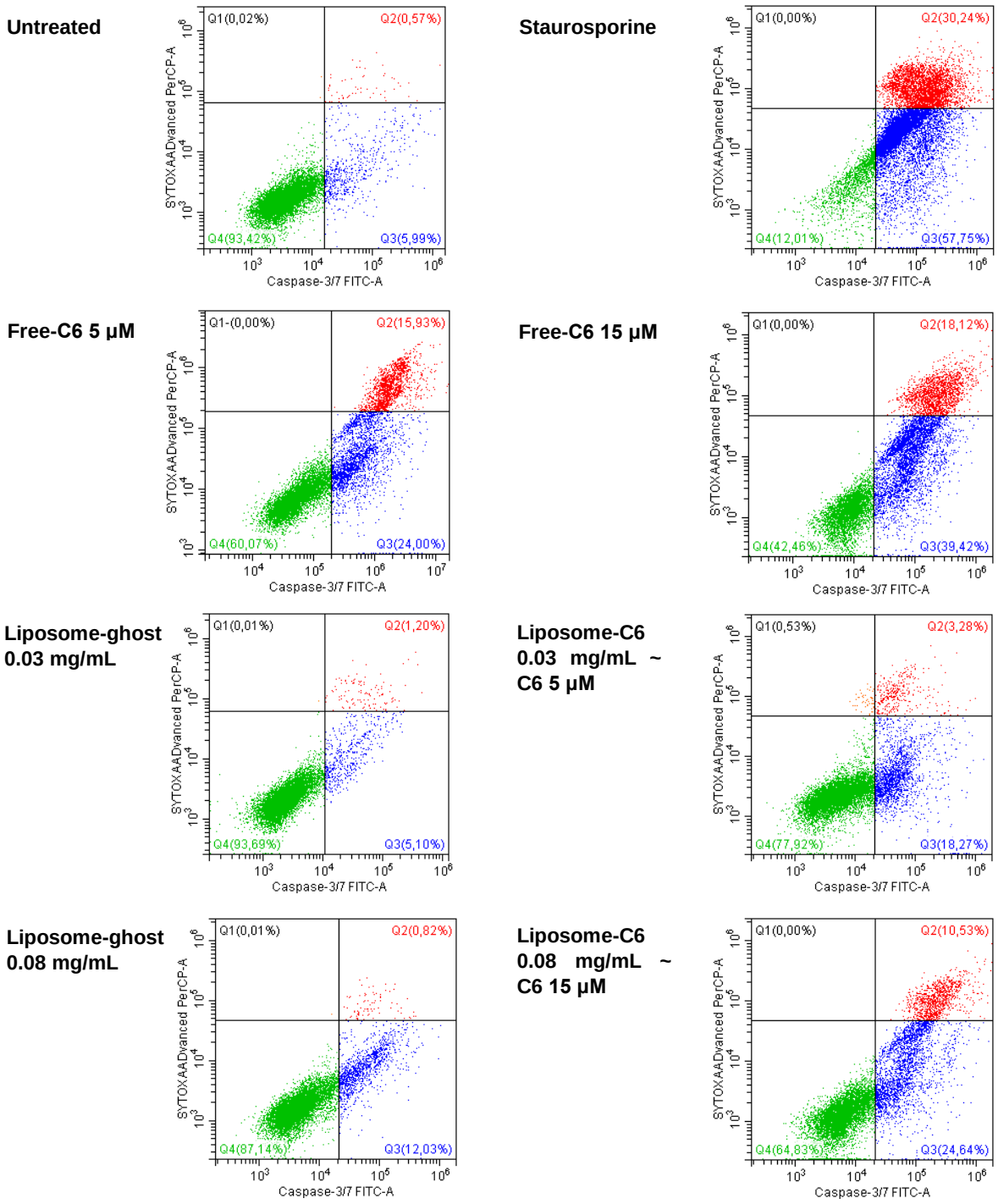

Figure S2. Representative flow cytometry dot-plots of MDA-MB-231 cells stained with CellEvent™ Caspase-3/7 Green Flow Cytometry Analysis Kit after 24h of treatment with staurosporine, free-C6 ceramide, and liposome with and without C6 ceramide.

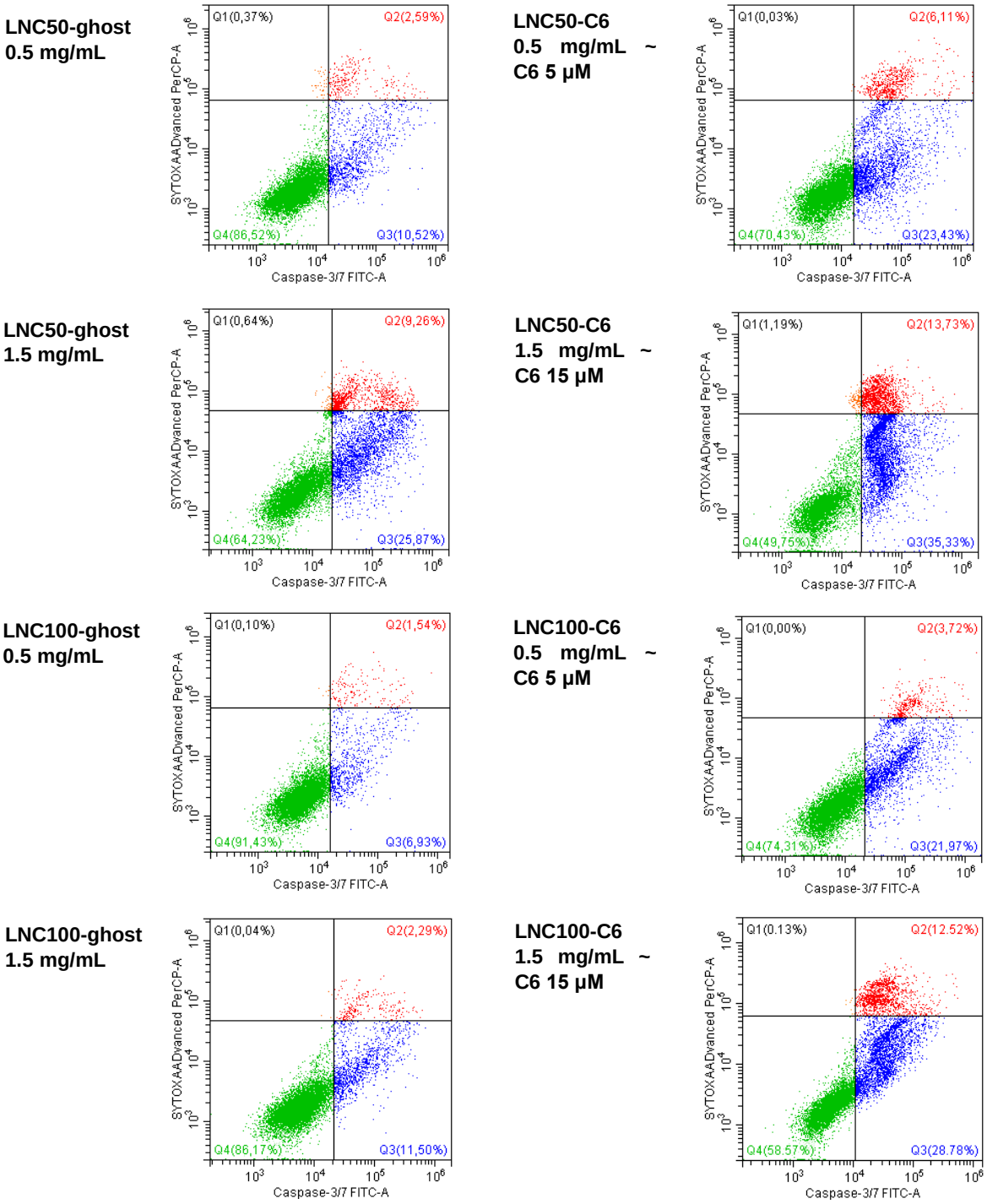

Figure S3. Representative flow cytometry dot-plots of MDA-MB-231 cells stained with CellEvent™ Caspase-3/7 Green Flow Cytometry Analysis Kit after 24h of treatment with LNCs with and without C6 ceramide.